International Journal of Disaster Risk Reduction 113 (2024) 104899

Contents lists available at ScienceDirect

International Journal of Disaster Risk Reduction

journal homepage: www.elsevier.com/locate/ijdrr

The effects of the Phlaegrean Bradyseism on building systems: Field research applied in Pozzuoli

Mariacarla Fraiese *, Veronica Vitiello, Roberto Castelluccio

D.I.C.E.A. - Department of Civil, Building and Environmental Engineering, University of Naples Federico II, Piazzale Vincenzo Tecchio 80, 80125, Naples, Italy

ARTICLE INFO

Keywords:
Bradyseism
Building risk
Building envelope
Vulnerability
Urban system
Risk management

ABSTRACT

The contribution presents the results of field research aimed at assessing the effects of the Phlaegrean Bradyseism phenomena on a building system located in the historic centre of Pozzuoli (Italy). The study falls within the scope of building façade vulnerability analyses conducted by the authors to support the Public Administration in managing bradyseismic emergencies.

Considering that the seismic-deformation phenomena connected to Bradyseism affect the performance and integrity of façade components, the research focused on studying its impact on the technical elements within the Technological Unit Classes of "Load-bearing Structure", "Enclosure", and "External Partition", which directly project onto the external environment and collectively constitute the Building Envelope. The methodology for impact assessment was developed by correlating data acquired from a monitoring system installed on the façade of a surveyed building with characteristic parameters related to seismic events and soil deformations in a specific reference period. The analyses conducted excluded any significant impact of these seismic-deformation forcings on the building's Load-bearing Structure, both in terms of displacements and damage. On the other hand, significant impacts were found on the technical elements of the building envelope, which, due to their lower resistance and ductility, represent a constant hazard for the exposed urban system's safety, configuring a Building Risk scenario.

1. Introduction

The contribution presents the results of field research aimed at assessing the effects of the Phlaegrean Bradyseism on a building system located in the historic centre of Pozzuoli (Italy), and the subsequent impacts on the urban system. The study is part of the building façade vulnerability analyses conducted by the authors to support the management of the bradyseismic emergency for the Public Administration.

Pozzuoli is located within the vast volcanic region of the Campi Flegrei (CF) in Campania, Italy. This area comprises a system of nested and resurgent calderas distinguished for millennia by its complex geological and seismological history, characterised by intense volcanic, tectonic and bradyseismic activity in constant evolution [1–6]. Bradyseism is a phenomenon related to the volcanic dynamics of the calderas and consists of a periodic uplift and subsidence of the ground, generating numerous seismic sequences of low-intensity and high-frequency during the ascending phases [2,7–9]. These events particularly affect the area of Pozzuoli's historic centre, where maximum deformation is recorded, and have influenced the city's history for many centuries [1,6,10–12]. The most recent bradyseismic crises occurred from 1969 to 1972 and from 1982 to 1984. During these periods, the ground uplift values, and the intensity of

* Corresponding author.
E-mail addresses: mariacarla.fraiese@unina.it (M. Fraiese), veronica.vitiello@unina.it (V. Vitiello), roberto.castelluccio@unina.it (R. Castelluccio).

https://doi.org/10.1016/j.ijdrr.2024.104899
Received 22 April 2024; Received in revised form 11 October 2024; Accepted 11 October 2024
Available online 11 October 2024
2212-4209/© 2024 The Authors. Published by Elsevier Ltd. This is an open access article under the CC BY license (http://creativecommons.org/licenses/by/4.0/).

the seismic swarms reached such levels within a short period that the historic centre had to be evacuated to protect the population from building damage and in anticipation of a potential eruption, which ultimately did not occur [2,7,11,13,14]. After a subsistence period of approximately 22 years, a new uplift phase has been underway since November 2005. As of March 2024, this phase has resulted in a ground uplift of about 122 cm in the Rione Terra area, with 89 cm of uplift occurring since January 2016, exceeding in absolute value the maximum historical deformation [15–17]. Unlike the two previous phases, the uplift velocity was on average low for most of the period considered, except for a few peaks, such as the one that occurred in 2012, which prompted the Civil Protection Department to declare a "*yellow alert*" level under the Campi Flegrei National Plan, which is still in force today [9,10,12,18–20]. Alert levels describe the state of volcano activity and are represented by four different colours (green, yellow, orange, red) indicating its possible evolution; the yellow level, in particular, indicates a state of potential disequilibrium of the volcano [21].

Since 2018, an increase in deformation velocity has been recorded, accompanied by a gradual rise in seismic activity, both in terms of frequency and intensity. This trend peaked in 2023, with over 2200 seismic events occurring in August and September alone, with a peak value of recorded Duration Magnitude of 4.2 ± 0.3, and an average uplift velocity value of approximately 15 ± 3 mm/month, causing significant concern among the population and all involved entities [11,16,18,22–25].

In the described context, the current configuration of the Bradyseism represents an atypical risk scenario, continuously impacting the urban system, understood as a set of buildings, infrastructures, and population. The soil deformation and associated seismic phenomena constantly stress all components of the system and contribute to a state of agitation among the population, strongly influencing daily life in the city of Pozzuoli [21,26–30]. These phenomena also have equally important impacts, including economic losses, interruption in essential services, and threats to people's safety [28,31,32]. These considerations highlight how bradyseismic activity represents a significant risk factor for the Phlegraean area, regardless of the probability of extreme eruptive or seismic events occurring.

At the building scale, Bradyseism constitutes a specific extensive risk scenario, exposing buildings to low-intensity and high-frequency solicitations [33,34]. This type of stresses includes, among others, hazards related to Climate Change (e.g., sudden heavy rainfalls, heat waves, wind loads), solicitations typical of highly urbanized contexts (such as interference with civil infrastructure systems), and environmental conditions [35–37]. These hazards continuously affect the building's technical elements, with significant effects on those pertaining to the Technological unit classes of "Enclosure" and "External Partition", rather than the "Load-bearing Structure". This is due to the fact that the former are particularly vulnerable to the direct impact of external hazards and suffer damage more readily and extensively as a result of frequent stresses over time, even if of low intensity [34,36–47]. This high vulnerability, related to their technological characteristics and state of preservation, leads to a decay in their performance characteristics, causing progressive deterioration and resulting in phenomena such as degradation and detachment, which constantly expose the urban system to potential falls of the elements or portion of them onto crowds [34,36,48,49]. In this regard, the technical elements of the building envelope that overhang public or private open spaces (such as cornices, cladding, gables, etc.), pose an additional and constant hazard for urban systems, configuring a specific Building Risk scenario [34]. This type of risk is indeed intended as the probability that a hazardous event, resulting from the vulnerability of the technical elements of the building envelope, can cause harmful effects on urban systems, in relation to the specific characteristics of the system's Vulnerability and Exposure [34,48]. This scenario often results in more frequent harmful effects compared to those related to the Load-bearing Structure, determining significant impacts even with respect to disasters [49–52].

The expertise gained by the authors through their involvement in supporting the Public Administration of the Campi Flegrei Municipalities, along with the studies carried out by the research group on Building Risk topics, emphasised the specific relevance of this risk scenario [34,53]. In this context, the technical elements of the building envelope not only pose a daily threat to the safety of the population, but can also obstruct escape routes, interrupt services, and compromise the performance and functional integrity of buildings, including those of strategic importance. This, in turn, amplifies the cascading effects associated with the occurrence of exceptional events.

The considerations outlined highlight the importance of assessing, together with the Bradyseismic Risk scenario for the Phlaegrean territory, also its impact on the built environment in terms of Building Risk. This is particularly crucial given the high vulnerability of the building systems and their façades, worsened by the seismic deformation forcings typical of the bradyseismic phenomena which, adding to other external hazards, significantly accelerate the degradation and disruption of the technical elements of the building envelope. Within the evaluation of Building Risk, the hazard deriving from this vulnerability is combined with the system's vulnerability, associated with the narrow structure of the urban centre, and the system's exposure, associated with the considerable population density that characterises it [35,48]. Despite the clear relevance of this issue, scientific studies in the literature have so far mainly focused on extreme risk scenarios, whether volcanic or seismic, analysing Bradyseism almost exclusively as a precursor phenomenon to potential eruptions and concentrating on its impact on Load-bearing Structures, while neglecting the effects on building systems as a whole, as well as the impacts on the entire urban system and the population, who must contend with the seismic-deformation phenomena daily [5,14,26,28,41,54].

This approach is reflected in the risk management policies adopted to date, which prioritise emergency planning over prevention measures and strategies for mitigating bradyseismic risk. These strategies should aim at reducing the vulnerability of urban systems at a multi-scale level, starting from the vulnerability of the technical elements of the building envelope, as well as implementing training and information programmes for the population [26,32,55,56]. This narrow focus undermines a comprehensive understanding and adequate perception of Bradyseism as an atypical risk scenario. A more holistic approach should consider the specific nature of deformation forcings and seismic phenomena and their potential impact on urban, economic, and social systems, regardless of the potential disaster events.

It is, therefore, of fundamental importance to deepen studies on the effects of bradyseismic phenomena on building and urban

systems, and to assess the additional Building Risk amplified by typical Bradyseism forcings on the urban system [13,16,22,29,30]. Such an approach provides the knowledge and tools necessary to reduce the vulnerability of the building envelope and, consequently, of the built environment. This ensures efficient prevention and mitigation measures for Building Risk, that should be coherent with the system of risks to which urban systems are exposed and supported by effective risk management and governance strategies aimed at enhancing overall urban resilience [57–60].

With this objective in mind, the contribution presents the results of experimental field research aimed at assessing the impact of solicitations typical of the bradyseismic scenario on the built environment, analysing the subsequent impacts on urban systems considering a period of reference marked by a significant series of low-intensity and high-frequency events.

The data processed in the framework of this study were collected through monitoring activities conducted by the authors as part of the support provided to the Public Administration for managing the emergency resulting from the collapse of a building's foundation system in the historic centre of the Municipality of Pozzuoli [61]. The building was evacuated in July 2023 by the Provincial Command of the Naples Fire Department to ensure public and private safety in the surrounding urban area and was subsequently subjected to safety interventions. After consolidating the subsoil by filling the cavities generated below the foundation level, effectively eliminating the causes of subsidence, a monitoring campaign was initiated. Its purpose was to record any further displacements or evolution of the cracking patterns related to Bradyseism forcings. The monitoring period included the period of maximum intensification of seismo-deformation events registered in August and September 2023 [23,24]. This coincidence provided the opportunity to record and correlate the information collected on the characteristic parameters of the seismic phenomena, detected by the Osservatorio Vesuviano [62], with the corresponding behaviour of the monitored building.

The data collected confirmed the stabilisation of the ground affected by subsidence and the building's substantial stabilisation even under the influence of bradyseismic forcings. However, the analyses conducted revealed the significant impact of Building Risk on the reference urban system: even after safety measures were implemented, the street remained closed to the public, and ground-floor commercial premises were shut down for a prolonged period, causing direct repercussions on the economic system and the population, as well as on the physical system at the building and infrastructure scale.

1.1. The classes of technological units investigated

Considering that seismic-deformation phenomena associated with Bradyseism have a significant influence on the performance and integrity of façade components rather than those of the Load-bearing Structure, the field investigation focused on examining all these technical elements to study and compare the different relevant impacts of the bradyseismic risk scenario. In the context of the proposed research, the technical elements of the building were broken down and classified according to the national standards in force, the UNI 8290 [63]. The classification outlined in the standard comprises three levels: 1) Class of technological units; 2) Technological units; 3) Classes of technical elements. This breakdown acknowledges the interconnection between the various components, transcending the conventional division between "structural" and "non-structural" elements, commonly found in the scientific literature [39,45,47,64]. The traditional classification does not adequately address the complexity of the building system nor provides a correct comprehensive view of the functionality and safety of each part of the system [38,65].

Applying the UNI 8290 classification, the building is instead intended as a "system" of different technical elements and, in this contribution, the Classes of technological units "Load-bearing Structure", "Enclosure" and "External Partition" are examined. The latter two directly overhang the external environment and, together, encompass all the Classes of technical elements that constitute the Building Envelope as a whole. The Building Envelope fulfils the purpose of protecting the building from external actions and defines the "boundary" between the building itself and its context. As already outlined in the introduction, it is essential to assess the impact of the bradyseismic scenario on these technical elements and, consequently, of the Building Risk they pose on urban systems [34,49,66–68].

1.2. Building displacement monitoring systems

Displacement monitoring systems are utilised to assess the behaviour of buildings in response to various external stresses, including accidental and cyclic loads as well as environmental conditions [69,70]. The significance of employing this type of instruments lies in their ability to provide real-time monitoring of building systems performance, allowing for an assessment of safety, functionality, and durability for all technical elements [14,70,71].

Monitoring systems generally consist of three main components: a data-collecting sensor, an acquisition and transmission unit, and a storage database [70]. Sensors can be categorised into two types: contact and non-contact, depending on whether they require direct installation on the element being investigated. Contact sensors include accelerometers, inclinometers, strain sensors, optical fibre sensors and global navigation satellite systems (GNSS) among others. Typical non-contact sensors, on the other hand, include vision cameras, laser Doppler vibrometers (LDV), radar, laser triangulation sensors (LTS), light detection and ranging (LiDAR) and total stations (TS) [70].

The potential and limitations of these systems depend on the type of sensor chosen and are primarily related to factors such as measurement accuracy, frequency range, cost, installation method, data processing or maintenance, susceptibility to interference, the type and range of displacement detected, and operating autonomy [14,70]. For contact systems, the accuracy of recorded data is closely linked to the number of sensors and their positioning on the survey surface. Proper positioning must be carefully designed in relation to the element being monitored and the amount of data required to evaluate its behaviour [14,70]. Therefore, the selection of the monitoring system to be employed cannot disregard a comprehensive understanding of the element under study and its context.

In the investigation conducted for this study, monitoring systems served as an essential tool for assessing the effects of Bradyseism-induced stresses on the building system. Given the nature and low-intensity of the seismic-deformation forcings analysed, the type and

amount of data provided by these contact monitoring systems were considered sufficiently accurate for the purpose of the study, as detailed in Section 2.2 [14].

2. Methodology

The methodological approach used for achieving the intended objectives was developed through the following steps: description of the application context of the field research (§ 2.1); acquisition and preliminary analysis of data related to inclinations and associated displacements (§ 2.2); selection and analysis of data related to seismic events (§ 2.3); data processing for comparison between seismic events and trend in displacement variations (§ 2.4). The conducted study relayed on the data acquired by the contact monitoring system, installed directly on the investigated façade, and the data related to the seismic events retrieved from the open-source GOSSIP© (GeneratOr of Serenade StatIc Pages) portal of the National Institute of Geophysics and Volcanology (INGV) [72]. The impacts on technical elements of the façade were assessed according to a critical analysis of the results obtained through the cited comparison.

The overall data analysis and processing cover the period from August 8, 2023, to January 23, 2024, which encompasses both the installation and removal dates of the monitoring system. The monitoring period spans the entire available dataset and includes the critical phase of intensified bradyseismic phenomena that occurred in August and September.

The reference period considered (less than one year) introduces limitations to the adopted procedure, as it does not allow for a full account of seasonal temperature variations and the effects on the trends of displacement, which may affect the interpretation of results related to proposed analysis. However, within the broader scope of the paper, it can still be functional to provide insights and to substantiate the study.

2.1. The application context of the field research

The analysed building is located within the area delineated by Goglia dei Mille street, Allumiera street and Corso Giuseppe Garibaldi (Fig. 1a). The latter represents one of the city's main thoroughfares and, considering its proximity to the Cumana railway station, experiences significant vehicular traffic, pedestrian congestion, and commercial activities.

Situated in the historical centre of Pozzuoli, the building's original layout is documented in historical charters, such as the land registry plan by Galli, A. dating back to 1874 [73]. According to the building age classification provided by the latest Census of Population and Housing conducted by ISTAT [74], which estimates the average construction age of buildings in the same census section, the building falls within the "*prior to 1919*" construction age class. Moreover, it is part of a complex comprising four aggregated buildings, all with masonry Load-bearing Structure, and it is a three-storey high, with an approximate height of 10 m, mainly used for residential purposes, except for the ground floor which is designated for commercial premises (Fig. 1b and c).

The studied façade in the present study is the one situated along Corso Garibaldi (Fig. 1). The technical elements analysed include an external wall with plastered and painted finishings, a masonry cornice with plastered and painted finishings, openings with plastered cornices and decorations, and balconies with intrados and frontedges with molded shapes and plastered and painted finishings. The construction technique of the balcony is undetectable, yet according to the prevalent one present in the area, it is hypnotised to be with steel girders, hollow core slabs, and reinforced slab on the intrados.

The urban context analysed falls within the C01 - Rione Terra compartment, as defined in a previous study by the authors on the vulnerability of the built environment in the Municipality of Pozzuoli (Fig. 2) [48].

The entire area, with a considerable population density (approximately 7320 inhabitants/km^2), has been classified as a High Building Vulnerability zone and is situated within the area of maximum bradyseismic ground deformation. This vulnerability was assessed in the study already mentioned and attributed to clusters of buildings with homogeneous characteristics in terms of

Fig. 1. The application context. a) Location of the surveyed building with the indication of the analysed façade on Corso Giuseppe Garibaldi, highlighted with a continuous red line; b) Investigated façade associated with the view "b"; c) Investigated façade associated with the view "c".

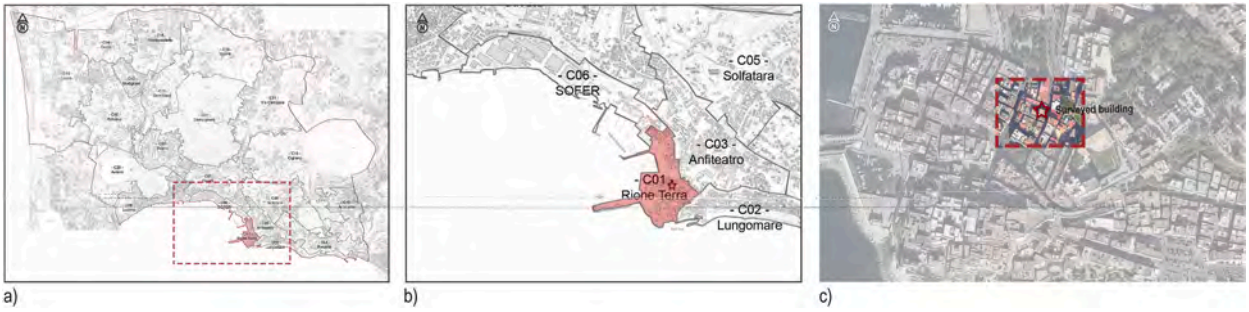

Fig. 2. The application context. a) The Municipality of Pozzuoli divided into the different compartments. The Rione Terra compartment is highlighted with a red hatching; b) Closer individuation of the C01 - Rione Terra compartment within the Municipality of Pozzuoli; c) location of the surveyed building in the Rione Terra compartment.

construction date, structure, and the typology of their technical elements, which together define specific Subcompartments. For each Representative Building, characteristic of its Subcompartment, the initial vulnerability analysis focused on the technical elements of the building envelope. A vulnerability score was first assigned based on construction techniques, their percentual incident on the envelope, and their positioning in height, using a numerical weighting algorithm. These factors were then combined with a first multiplier factor accounted for the state of preservation of these elements, and a second one related to System vulnerability, in terms of the ratio of building height to street width, and to Population Exposure, in terms of Housing Density. This qualitative-numerical analysis made it possible to determine the Building Vulnerability value, which, assigned to the Subcompartments, was expressed on a scale of 1–4: Class 1 Moderate Vulnerability; Class 2 Medium Vulnerability; Class 3 High Vulnerability; Class 4 Very High Vulnerability [48]. The Subcompartment where the analysed building is located is characterised by buildings built before 1964 (according to the classification used in the cited study [48]), primarily with masonry load-bearing structures. The prevalent construction techniques for the envelope's technical elements are similar to those of the analysed building, featuring plastered and painted finishings, along with balconies and cornices on at least two-to-three façades, all in a fair state of preservation (information dated to the cited study). When these factors were combined with the Building Height-to-Street width ratio and the Subcompartment's Housing Density, the previously mentioned High Vulnerability Class was assigned.

Following the emergence of a significant increase in a crack pattern on the façade and disruption of the sidewalk underneath, the Provincial Command of the Naples Fire Department urgently ordered the evacuation of the building and those directly adjacent to it in July 2023 (Fig. 3) [61]. In response to the emergency management support required by the Public Administration, immediate diagnostic investigations were aimed at understanding the causes of the observed phenomena and defining the necessary intervention measures.

The crack pattern in question, identified in Fig. 3 in red, includes diagonal cracks located on the cantonments of the building, and sub-vertical cracks in the central portions of the façade.

After the initial diagnostic investigations, this type and distribution of cracks were considered compatible with an active kinematism of the building. It was attributed to the progressive subsidence of the foundation-soil system, caused by the formation of large cavities beneath the left cantonment of the building, due to surface water leaks.

On the investigated façade, other crack patterns and degradation and damage phenomena have been observed, not related to the described kinematism and already existent before the occurrence of the emergency. These are indicated in Fig. 3 in green and include: a

Fig. 3. Graphical representation of the crack patterns observed on the investigated façade and identification of the degradation and damage phenomena observed on the building envelope. In red are the anomalies clearly associated with the subsidence of the foundation soil; in green are the anomalies not directly attributable to the subsidence.

widespread lesion pattern on the external wall, with lesions that do not seem to be localised and have no prevalent direction; more or less severe swellings and detachments of the finishings; other minor superficial anomalies such as chromatic alteration, staining, colatura and other superficial deposits. These same superficial anomalies are also observed on the cornice and the intrados and front-edge of the balconies (Fig. 3).

The damage of these elements determined a hazard for the urban context associated with the probability of their detachment and fall onto crowds. The direct consequences of this hazardous condition resulted in the prohibition of both vehicular and pedestrian traffic along the road axes facing the building, enforced to ensure public and private safety.

Following safety interventions, which involved filling the cavities with cohesive material of a specific weight equivalent to the original soils, a continuous contact monitoring system was set up with the installation of inclinometers. The objective was to validate the effectiveness of the safety measures adopted and to assess potential evolutions of the observed prevalent cracks, also due to the potential effects of bradyseismic phenomena on the building's behaviour. In the proposed study, to monitor the other types of lesions and anomalies, an analysis of the previous state of conservation of the technical elements of the building was conducted.

2.2. Acquisition and analysis of data related to inclinations and associated displacements

The installation of the monitoring system and the related data acquisition were carried out with the support of TECNO IN S.p.A., a company specialised and certified in diagnostic surveys on the built environment. Three fixed biaxial surface inclinometers were installed on the investigated façade, connected to a stand-alone acquisition unit.

The inclinometers were installed in the horizontal direction by means of an anchor plate fixed to the building façade, according to the diagram depicted in Fig. 4a.

Fig. 4b shows the reference system adopted by the monitoring system for data reading and interpretation.

The first transducer (INCL_1) was positioned on the cantonment where the prevailing foundational failure has been identified, at an elevation of 10 m (Fig. 5a). The other two transducers (INCL_2, INCL_3) were located on the opposite cantonment, vertically aligned, and placed at elevations of 10m and 6m, respectively (Fig. 5b). The number of inclinometers and their positioning were chosen to ensure effective coverage of key areas of the building and to obtain an adequate assessment of its behaviour in response to external solicitations [14,70,75].

The acquisition unit (model UAD MS-16) was installed directly on the façade (Fig. 5c) and was equipped with a high-capacity battery, continuously powered by a 50W solar panel, to ensure that the system could operate even during night-time and on cloudy days.

The transducer model used (SCA128T) features Micro Electro Mechanical Systems (MEMS) sensors enclosed in waterproof aluminium enclosures. These sensors are capable of transmitting acquired data up to a distance of 2 km and measuring inclination variations in the range of $\pm 10^{\circ}$ relative to the zero established on the reference surface at the time of installation. The resolution, defined as the smallest detectable variation within the sensor's measuring range, is 0.01°; the measurement accuracy, which accounts for combined errors including linearity, repeatability, hysteresis, zero deviation, and horizontal axis error under normal temperature conditions (25 °C), is 0.03°. These instrumental characteristics ensure that the measurements have appropriate resolution and stability for typical usage conditions.

This type of sensor is commonly used to measure changes in inclination in civil structures where displacements with rotational components are expected. Among its various applications, it is frequently used in monitoring buildings affected by landslides or earthquakes, making it well-suited for the specific objectives of this study.

The sensor operates on the capacitive micro-pendulum principle, which leverages the variation in electrical capacity induced by the movement of a small pendulum between two electrodes inside the sensor. Fig. 6 shows the operating principle of the sensors, with U_L and U_R representing the tensions between the left and right plates of the pendulum and the respective electrodes. When the sensor's inclination deviates from its initial position, the earth's gravitational component influences the pendulum in motion, altering the distance between the capacitor plates.

This change in distance results in a corresponding alteration in the electrical capacity of the system, which affects the U_L and U_R

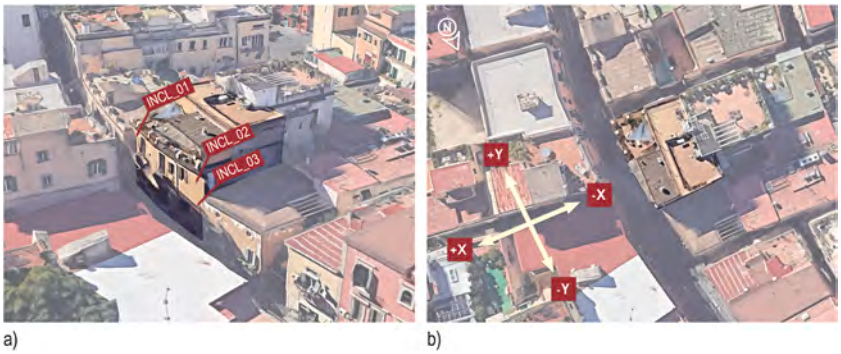

Fig. 4. Location of the monitoring system. a) Aerial view of the surveyed building and indication of the positioning scheme of the inclinometers. b) Aerial photogrammetry of the area with identification of the reference system used by the monitoring system.

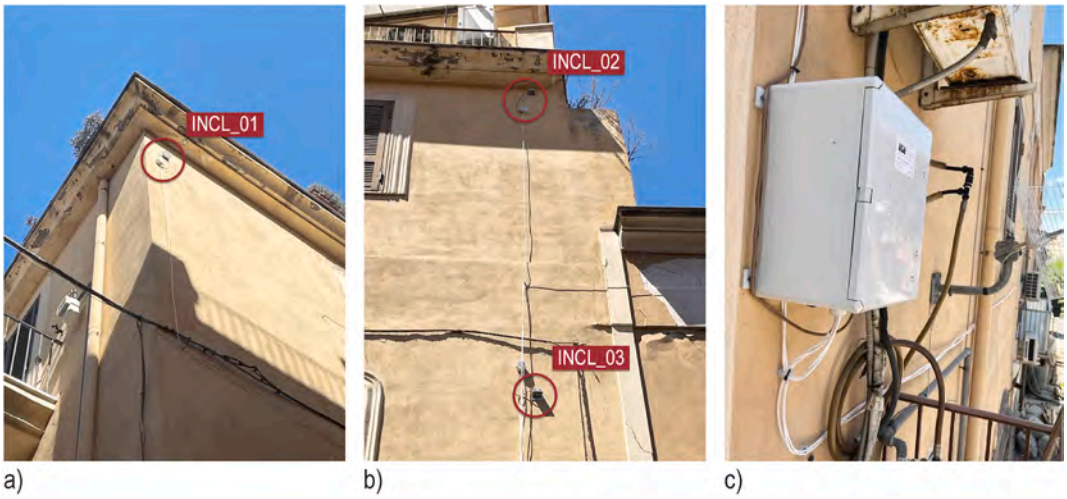

Fig. 5. Details of the monitoring system components. a) Positioning of transducer INCL_1. b) Positioning of transducers INCL_2 and INCL_3; c) Positioning of the acquisition unit.

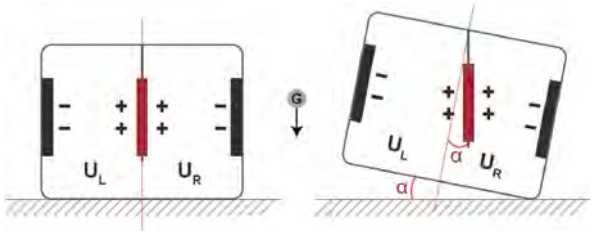

Fig. 6. Schematic representation of the operating principle of inclinometers.

values. The relationship between the variation of these two values depends on the inclination angle **α** of the sensor with respect to the reference surface (Eq. (1)) [69,76,77].

$$\alpha = f\left(U_L; U_R\right) \tag{1}$$

The sensors, therefore, allow for a measurement of the angular values of building inclination relative to the reference surface on which they are installed. According to the reference system adopted in this analysis, they provide inclination values in the two mutually orthogonal planes XOZ and YOZ (Fig. 4b). Simultaneously, they also record the external temperature values at each measurement instants. The acquisition unit records the information with a transmission frequency of 30 min and transmits it in real-time to a cloud server for storage. Data access is available via the personal web portal of the monitoring company.

In the reference period under consideration, from the first measurement at 12:05 a.m. UTC on August 8, 2023, corresponding to the activation of the inclinometers, to the last measurement at 11:56 p.m. UTC on January 23, 2024, the system carried out a total of 7652 measurements. Table 1 shows the number of measurements taken per each month.

Below, for each installed inclinometer, the diagrams of the inclination variation in the XOZ (Fig. 7a) and YOZ (Fig. 7b) planes, expressed in sexagesimal degrees, are shown. At times, interpreting data collected through monitoring systems of this type can be complex due to excessive temperature variations occurring during the observation period [14,78]. Therefore, to account for possible influences on the changes in recorded inclinations, the temperature trend, expressed in degrees Celsius, is also overlaid on the diagrams.

Table 1
Number of measurements taken by the monitoring system during the entire reference period and per each month.

Period considered		Measurements taken
Entire Reference Period	*(August 08, 2023 – January 23, 2024)*	*7652*
August	*(August 08, 2023 – August 31, 2023)*	*1128*
September	*(September 01, 2023 – September 30, 2023)*	*1443*
October	*(October 01, 2023 – October 31, 2023)*	*1488*
November	*(November 01, 2023 – November 30, 2023)*	*1440*
December	*(December 01, 2023 – December 31, 2023)*	*1468*
January	*(January 01, 2024 – January 23, 2024)*	*685*

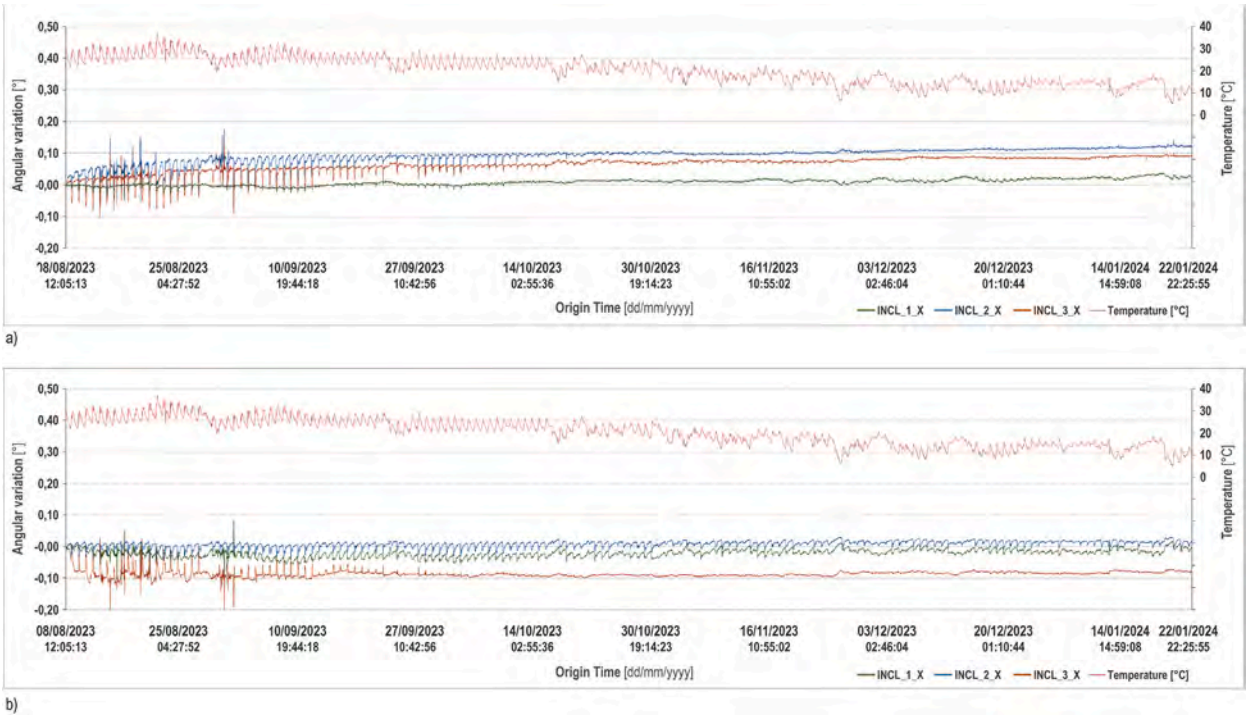

Fig. 7. Results of inclinometer monitoring. a) Trend of inclination variation registered by inclinometers in the XOZ reference plane; b) Trend of inclination variation registered by inclinometers in the YOZ reference plane. Both diagrams also include a graph depicting the external temperature trend.

In detail, the temperature variation from August to September ranged between 19 °C and 30 °C, with average temperatures of approximately 28 °C for August and 25 °C for September. In August, there were some peaks during which temperatures exceeded 30 °C, with a maximum of 37 °C recorded on August 21, 2023, around noon. There was a relatively rapid decrease in temperature, concentrated over a few days, between the end of August and the beginning of September, followed by stabilisation around the average September values. From October to January, temperatures ranged between 10 °C and 25 °C. During this period, there were no significant peaks, while there were some notable drops between October 15 and 17 where the temperature dropped from 24 °C to 15 °C; between November 24 and 26, with the temperature changing from 19 °C to 7 °C, and from January 19 to 21 with a change from 16 °C to 5 °C, the latter being the minimum temperature value for the entire reference period. Considering the sensitivity error associated with thermal variations for the sensors used, it can be assumed that the observed trend remained within a reliable range to guarantee the accuracy of the collected data.

The recorded data were processed to derive the relative displacements. In detail, the displacement associated with the registered inclination can be obtained using the trigonometric relationship existing between the inclination angle (α) expressed in radians; the distance along the inclination, corresponding to the height of the inclinometer considered from the reference 0 point (H); and the horizontal distance, corresponding to the relative displacement (d) (Eq. (2)).

$$\tan \alpha = \frac{d}{H} \tag{2}$$

The value of the displacement along the two directions of the X and Y axes, denoted as d_x and d_y, can therefore be derived using Eq. (3):

$$d(\alpha) = \tan \alpha \text{ x H} \tag{3}$$

This involves converting the angular inclination values from degrees centigrade to radians and placing the height values of each inclinometer. The resulting diagrams, showing the trend of variation of the relative displacement values along the X and Y components, expressed in centimetres, are presented in Fig. 8. Considering the reference system adopted (Fig. 4b), positive/negative inclination values along the X component can be associated with horizontal displacements of the reference plane in the west/east direction. Conversely, positive/negative values along the Y component can be correlated with rotations in the south/north direction.

By studying both the trends in the displacement variations values and their amplitude, as well as the average cumulative displacements over time, the following preliminary considerations can be deduced. This analysis is aimed at describing the obtained diagrams and is prodromic for the subsequent phases, deferring their elaboration to the results sections.

The INCL_1 inclinometer (Fig. 8a), shows almost no variations along the X component, while slightly more pronounced variations are observed on the Y component throughout the entire reference period. In both cases, the variations follow a stabilised cyclical

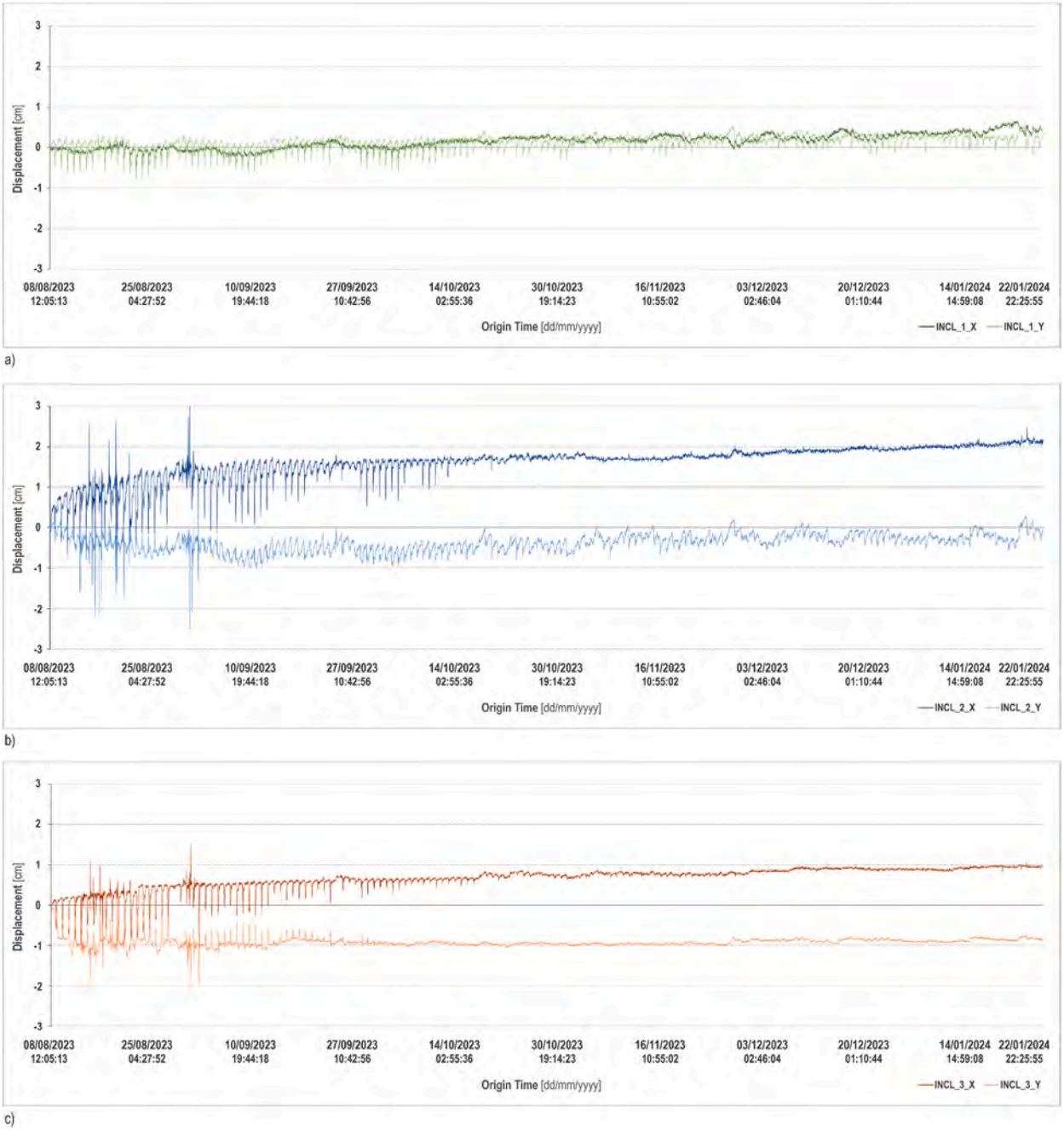

Fig. 8. Trend of displacement variation along the components X and Y. a) Variation of displacement values for INCL_1; b) Variation of displacement values for INCL_2; c) Variation of displacement values for INCL_3.

pattern with no sudden peaks or notable changes in their amplitude, indicating an absence of significant displacement variations along either component. Considering the cumulative trend of displacements, it can be observed that the variations fluctuate in a range close to zero until the beginning of October. After this point, the variations continue to follow a regular pattern, although slightly deviating from the zero axis, accumulating an average final displacement ($d_{x,med}$, $d_{y,med}$) of less than 0.2 cm along both positive axes (south-west directions) (Table 2), which can be considered close to null. The maximum displacement value along the X component ($d_{x,max}$) was recorded in January (Table 2); it is close to the final average trend previously estimated and follows the same positive direction, appearing to be consistent with the overall trend analysis shown in the diagram. The maximum displacement value along the Y component ($d_{y,max}$), recorded in the middle of August, is slightly higher and in the negative direction (Table 2); however it is not high enough to be considered a significant peak, and the different direction is coherent with the overall trend of variations that occurred in

Table 2
Maximum recorded values of displacements [cm] along the X and Y components for each inclinometer, along with the corresponding measurement dates and average recorded values of displacement over the reference period. Negative or positive signs indicate the direction of the displacements along the two components relative to the reference system employed.

Maximum displacement values			
Inclinometer	**Components**	**Displacement *[cm]***	**Time-Origin *[dd/mm/yyyy] [UTC]***
INCL_1	$d_{x,max}$	*(+)0,66*	*January 19, 2024 10:21:40*
	$d_{y,max}$	*(−)0,80*	*August 22, 2023 09:09:14*
INCL_2	$d_{x,max}$	*(+)3,07*	*August 30, 2023 23:07:45*
	$d_{y,max}$	*(−)2,51*	*August 30, 2023 23:07:45*
INCL_3	$d_{x,max}$	*(+)1,53*	*August 30, 2023 23:07:45*
	$d_{y,max}$	*(−)2,16*	*August 14, 2023 19:15:46*
Inclinometer	**Components**	**Average displacement values *[cm]***	
INCL_1	$d_{x,med}$	*(+)0,15*	
	$d_{y,med}$	*(+)0,13*	
INCL_2	$d_{x,med}$	*(+)1,61*	
	$d_{y,med}$	*(−)0,37*	
INCL_3	$d_{x,med}$	*(+)0,67*	
	$d_{y,med}$	*(−)0,90*	

August.

The INCL_2 and INCL_3 inclinometers (Fig. 8b and c) exhibit significant variations along both components until the end of August, still following a prevalent cyclical pattern. In this same period few notable changes and peaks in their extents can be observed, some of them corresponding to maximum displacement values $d_{x,max}$ and $d_{y,max}$ recorded for both inclinometers (Table 2). These values show a significant deviation from the August trend as well as from the overall trend observed over the entire reference period. Thereafter, the variations are still notable, but progressively decrease over the reference period, assuming eventually an oscillatory trend with almost no variation, yet stabilised within a range of values distinct from the reference zero. This indicates the presence of a permanent cumulative displacement that occurred over time, which for INCL_3 is evident along both components, while for INCL_2 it is more pronounced along the Y component. In detail, the average final displacement cumulated for INCL_2 is about 1.6 cm along the +X axis (east direction) and 0.4 cm along the -Y axis (north direction); while for INC_3 there is an average final displacement of about 0.7 cm along the +X axis (east direction) and 0.9 cm along the -Y axis (north direction) (Table 2).

In general, the analysis of variations and cumulative displacement behaviour for INCL_1 shows minimal fluctuations and changes in values. INCL_2 and INCL_3 exhibit similar trends among them, which differ notably from the one observed for INCL_1. In this case, more pronounced variations are observed, specifically from August to the beginning of October. After this period, the analysis leads to the same considerations made for INCL_1, with no more significant fluctuation in the displacement variations, but with a slightly more significant extent of the permanent displacement cumulated over time. Moreover, INCL_2 and INCL_3 have undergone prevalent displacements along the +X and -Y axes (northeast direction), while for INCL_1, the final displacements are along the +X and +Y axes (southeast direction).

2.3. Selection and analysis of data related to seismic events

Once data on displacement variations have been acquired, the subsequent step focuses on the selection and analysis of seismic events that occurred during the same reference period.

The open-source GOSSIP© (GeneratOr of Serenade StatIc Pages) portal provided by the National Institute of Geophysics and Volcanology (INGV) [72] was used for event selection. This portal, which is updated in real-time, relies on the information from the SERENADE© database, which comprehensively documents all earthquakes recorded by the Permanent Seismic Network of multi-parameter monitoring, managed by the Vesuvius Observatory, and occurred in the relevant areas of responsibility (Tirreno Litorale Domizio, Campi Flegrei, Vesuvio, Ischia, Golfo di Napoli and Penisola Sorrentina) [11,62,72,79].

During the reference period from August 8 to January 23, a total of 2936 earthquakes were documented. Table 3 presents the monthly distribution of these earthquakes, clearly showing the extent of the intensification of bradyseismic phenomena between August and September, with a significant difference in the number of earthquakes during these two months (70 % of the total) compared to those occurred from October to the 23rd of January.

Table 3
Number of earthquakes occurred per each month of the reference period.

Month considered		**Number of earthquakes**	**% of the total**
August	*(August 08, 2023 – August 31, 2023)*	*940*	*32 %*
September	*(September 01, 2023 – September 30, 2023)*	*1106*	*38 %*
October	*(October 01, 2023 – October 31, 2023)*	*553*	*19 %*
November	*(November 01, 2023 – November 30, 2023)*	*159*	*5 %*
December	*(December 01, 2023 – December 31, 2023)*	*76*	*2 %*
January	*(January 01, 2024 – January 23, 2024)*	*102*	*3 %*

Among these, events with magnitudes less than $M_d = 1.2 \pm 0.3$ were omitted to focus on earthquakes with substantial intensity in terms of effects on building systems. This refinement resulted in the identification of 161 earthquakes. To streamline the analysis and concentrate on relevant events within the studied area, the results of this initial selection were further narrowed considering only those earthquakes with hypocentres within a 3 Km radius of a designated Center Point, selected in the vicinity of the building (Fig. 9).

The decision not to centre the designated Center Point on the building's location was made to encompass the Solfatara-Pisciarelli area within the selection radius, as it recorded the highest number of earthquakes during the period considered, thereby giving an additional dimension to the selection process [16,23,24]. From the 161 earthquakes previously identified, a new selection of 131 events was thus obtained. Further refinement excluded earthquakes with epicentres located within the Gulf of Pozzuoli, which might have had lesser impacts on the built environment, leading to a final selection of 128 earthquakes.

In Annex A, detailed data on the main location parameters are provided for each event, including Time-Origin (date and time) in UTC zone; Location (epicentre location), in decimal degrees; Depth of hypocentre, in km; Duration Magnitude (M_d).

Fig. 10 illustrates the geographic distribution of the 128 selected seismic events within the designated survey area, categorised graphically according to the two parameters of hypocentre location depth and Duration Magnitude.

Fig. 11a illustrates the daily distribution of the 128 selected seismic events throughout the reference period. It also highlights time intervals of increased seismic activity, identified as "clusters" of earthquake events, in which multiple events occurred close together. Over the entire reference period, two distinct clusters of seismic activity were observed, both during the two months of the phenomena intensification. The first cluster spans from August 15 to 21, during which 34 earthquakes were recorded, accounting for 81 % of the August events and 27 % of the total. Notably, the highest number of daily earthquakes was recorded on August 18, with 19 occurrences. The second cluster was observed from Sept. 22 to September 29, encompassing a total of 43 events, which accounted for 86 % of September events and 34 % of the total, with 12 earthquakes recorded on September 26 alone. During the months from October to January, seismic activity decreased rapidly, with only 20 significant events recorded in October, 13 in November, 2 in December and only 1 in January. These time intervals, as well as those falling outside the two clusters, are categorised as periods "*of minor seismicity*".

Fig. 11b depicts the distribution of the events across their various hypocentre depth intervals, highlighting the percentages of events within each depth range. Consistent with the characteristics of bradyseismic phenomena, all earthquakes exhibit shallow depths, with the prevalent distribution varying between 0.2 km and 3 km.

Regarding the distribution of Duration Magnitudes, illustrated in Fig. 11c, of the total 128 earthquakes, 93 have values between 1.5 and 2; 27 have intensities ranging from 2 to 3; while 8 events show magnitude greater than 3. The most significant event occurred on September 9, 2023, at 01:35 a.m. UTC, with a Duration Magnitude of 4.2 ± 0.3. So far, this event represents one of the most energetic recorded since the beginning of the current unrest phase and in the last 40 years. Although the magnitudes of these earthquakes may appear low compared to typical thresholds considered in seismic assessments [80,81], they are located almost entirely in the Municipality of Pozzuoli and are characterised by particularly shallow hypocentre depths. This results in more intense local effects on the affected building systems, warranting a lower magnitude threshold value to be considered [82,83].

2.4. Data processing for comparison between seismic events and trends of displacement variations

The last phase of the methodology consisted of processing the data sets collected in the previous phases to elaborate the comparison between seismic events and the trends of displacement variation.

Fig. 9. Identification of the chosen survey area within a 3 km radius of the Centre Point. The location of the Centre Point (Lat: 40.83023; Long: 14.13216) and the respective location of the surveyed building are highlighted - Adapted from: Google Earth, Image © TerraMetrics, Data SIO, NOOA, U.S. Navy, NGA, GEBCO.

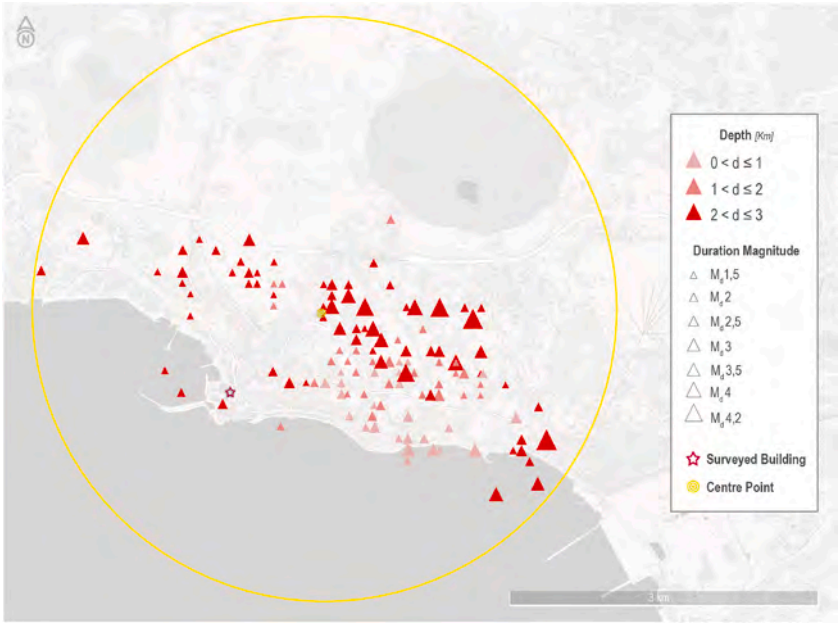

Fig. 10. Geographical location of the 128 selected seismic events. The coloured scale indicates the depth distribution, while the symbol size is proportional to the Duration Magnitude.

Below is a description of the two different analysis methods used for the comparison.

The first method involved comparing individual seismic events with the displacement variations recorded at the instants of their occurrence. The aim is to identify potential correlations between the events and the changes in trends of displacement variations analysed in Section 2.1, to eventually assess the localised impacts on the building.

In this analysis, only the most significant earthquakes in terms of impact on the local response were considered. This selection includes events with a Duration Magnitude of at least $M_d \geq 2.8$ and those with epicentre located within a radius of 1 km from the surveyed building. This distance represents the limit beyond which seismic phenomena associated with Bradyseism show a significant level of attenuation. By applying these criteria to the 128 events previously identified (§ 2.3), a total of 38 seismic events were selected, comprising 20 and 18 earthquakes respectively (Table 4).

Considering that the inclinometer sampling frequency is set at 30-min intervals, there may not always be temporal alignment between the measurement instants and the occurrence of seismic events. Therefore, the analysis of the displacement variations' diagrams is conducted within suitable time intervals to encompass the instants immediately preceding and following the events. Indeed, for the purpose of this study, the 30-min sampling is still considered suitable to adequately capture and examine both general and cumulative effects on the trends of displacement variations patterns due to seismic events.

Data on displacement values and variations registered by each inclinometer in time intervals close to the occurrence of each event are presented in Annex B of the Supplemental Files.

At the time of each earthquake, the extent of displacements and the direction and amplitude of variations were analysed. The first set of data, referring to the extent of displacements, is first compared to the maximum d_{max} displacement values observed (Table 2) to examine any correlation between the two phenomena. This is followed by a comparison to the average d_{med} displacement values recorded during different selected time intervals (Table 5), which include the entire reference period, the three distinct periods identified as "*minor seismicity*", and the time intervals associated with clusters of seismic activity (§ 2.3). The second set of data, related to the displacement variations, is compared to the average Δd_{med} and maximum Δd_{max} displacement variations values registered over the entire reference period, as well as over the other time intervals considered, to assess if they are coherent with the relevant trends observed (Table 5). The method involves comparing both data sets with values from the entire reference period, as well as with those from the other mentioned time intervals to account for the full range of different conditions to which the building was subjected.

In both cases, if anomalies in the extents of displacements, as well as in the direction and amplitude of variations registered before and after the seismic event are identified, a comprehensive analysis of the data in relation to the overall trend of displacement variations is conducted to determine whether they could be associated with the occurrence of the event itself.

The second method involved examining the trend of displacement variations in correspondence with the clusters of seismic events previously identified (§ 2.3) and comparing them with the trends related to the period of *minor seismicity* and with the general trend observed over the entire reference period. In this case, the analysis aims at identifying possible correlations between the frequent stresses induced by the families of closely occurring events and possible differences in the trends observed in the respective time intervals of occurrence, to obtain an assessment of the cumulative effects on the building. For this purpose, the average displacement values d_{med} and the amplitude of the average variations Δd_{med} recorded during the clusters are compared to those observed during the other time intervals considered, to detect possible differences in the temporal patterns and persistence indices (Table 5).

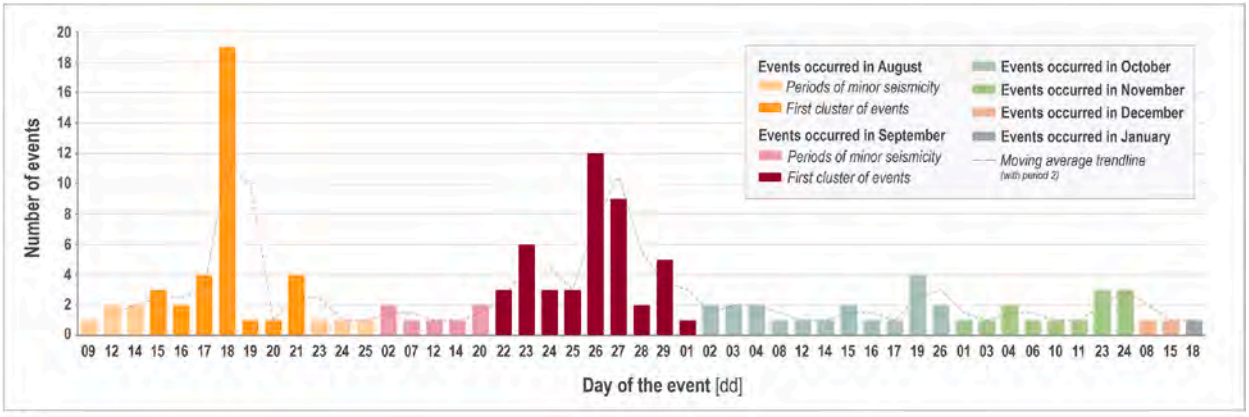

a)

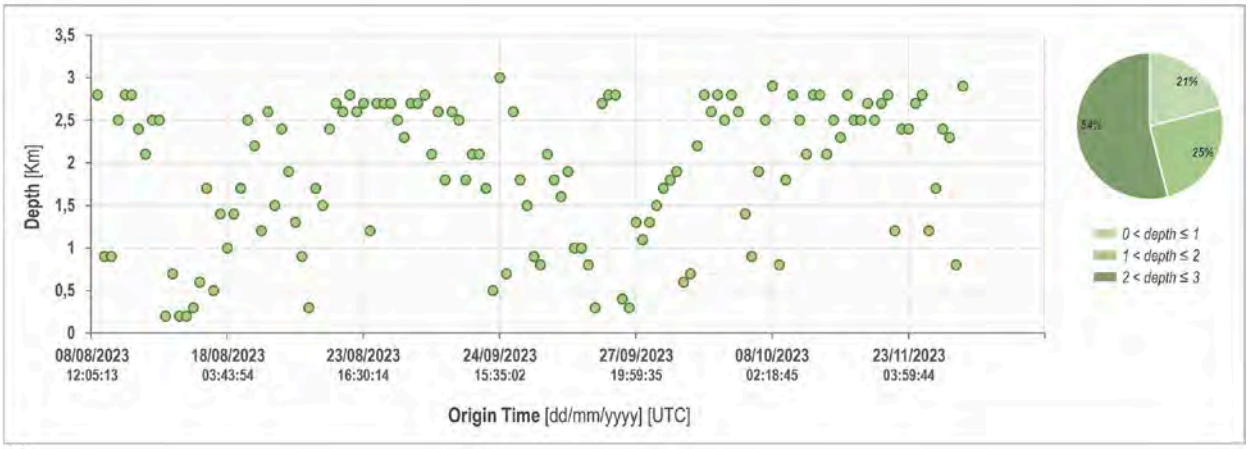

b)

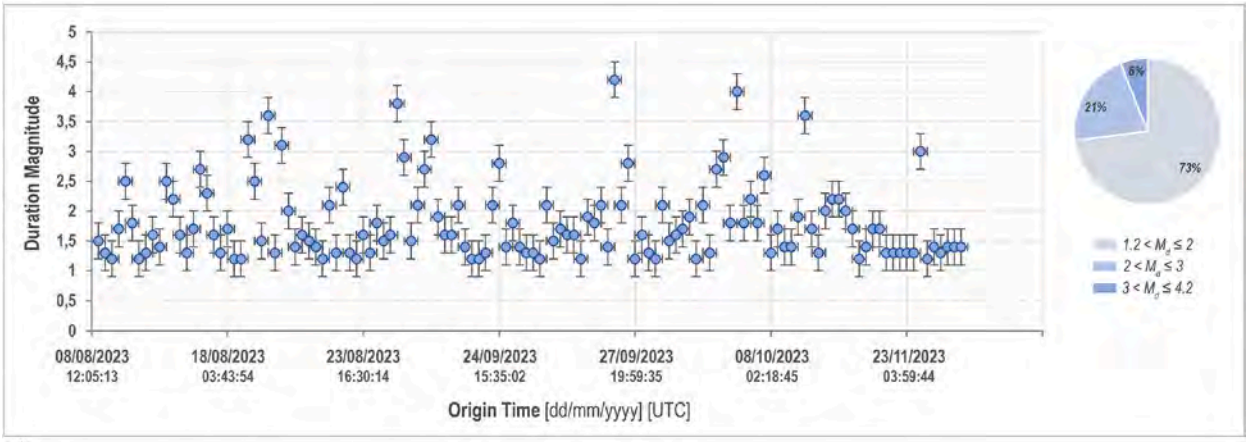

c)

Fig. 11. Trends of the main seismological parameters of the 128 selected seismic events during the reference period. a) Seismic events frequency per day. The trend line is used to evaluate the trend in the temporal data regarding the number of seismic events; b) Depth distribution of the selected events during the reference period. The pie graph shows the incidence of the identified depth ranges in relation to the total number of events; c) Distribution of the Duration Magnitudes of the selected events during the reference period with the relative vertical error bars of ±0.3. The pie graph shows the incidence of the identified magnitude ranges in relation to the total number of events.

Fig. 12 shows the diagrams of the trends in displacement variations for the three inclinometers along both components X and Y. For graphical comparison, on the same graph are indicated the 38 seismic events selected for the first analysis method at their respective times of occurrence and classified according to their Duration Magnitude, as well as the different time intervals corresponding to the two identified clusters of events considered for the second method of analysis are indicated as well.

Table 4
Main location parameters of the 38 seismic events and their distance from the surveyed building. Red indicates events with a magnitude greater than or equal to 2.8; blue indicates events with epicentre located within a 1 km radius of the surveyed building.

Date [dd/mm/yyyy]	Time [UTC]	Latitude [DD]	Longitude [DD]	Depth [Km]	Magnitude [M_d]	Distance from the building [m]
14/08/2023	22:46:51	40.8370	14.1037	2.8	2.5 ± 0.3	226
16/08/2023	08:22:07	40.8232	14.1155	2.5	1.6 ± 0.3	60
16/08/2023	08:27:09	40.8252	14.1137	2.5	1.4 ± 0.3	81
17/08/2023	03:59:57	40.8180	14.1450	0.2	2.5 ± 0.3	240
18/08/2023	00:01:28	40.8188	14.1505	0.6	2.7 ± 0.3	293
18/08/2023	04:09:59	40.8268	14.1480	2.5	3.2 ± 0.3	268
18/08/2023	04:10:30	40.8277	14.1517	2.2	2.5 ± 0.3	306
18/08/2023	04:18:05	40.8315	14.1375	2.6	3.6 ± 0.3	181
18/08/2023	04:22:49	40.8297	14.1387	2.4	3.1 ± 0.3	185
25/08/2023	01:24:09	40.8250	14.1267	2.7	1.8 ± 0.3	56
07/09/2023	17:45:28	40.8313	14.1465	2.5	3.8 ± 0.3	263
12/09/2023	02:28:50	40.8280	14.1392	2.3	2.9 ± 0.3	184
20/09/2023	22:54:29	40.8158	14.1582	2.8	2.7 ± 0.3	374
22/09/2023	09:01:59	40.8315	14.1432	2.1	3.2 ± 0.3	233
22/09/2023	21:46:10	40.8228	14.1203	2.6	1.9 ± 0.3	12
23/09/2023	03:18:56	40.8242	14.1283	2.5	2.1 ± 0.3	69
23/09/2023	12:29:56	40.8245	14.1302	2.1	1.2 ± 0.3	88
23/09/2023	12:42:22	40.8245	14.1305	2.1	1.2 ± 0.3	91
23/09/2023	13:08:33	40.8315	14.1263	1.7	1.3 ± 0.3	98
24/09/2023	15:35:02	40.8140	14.1537	3.0	2.8 ± 0.3	334
26/09/2023	01:34:55	40.8238	14.1340	0.8	1.2 ± 0.3	125
26/09/2023	03:54:56	40.8240	14.1342	1.0	1.6 ± 0.3	127
26/09/2023	06:50:22	40.8255	14.1345	1.0	1.2 ± 0.3	132
26/09/2023	13:55:16	40.8242	14.1320	0.8	1.9 ± 0.3	106
27/09/2023	01:35:34	40.8192	14.1590	2.8	4.2 ± 0.3	377
27/09/2023	09:16:18	40.8187	14.1423	0.3	2.8 ± 0.3	212
27/09/2023	20:25:37	40.8260	14.1338	1.1	1.6 ± 0.3	127
27/09/2023	23:14:30	40.8200	14.1277	1.8	1.5 ± 0.3	69
28/09/2023	14:42:03	40.8243	14.1317	1.9	1.6 ± 0.3	103
28/09/2023	18:38:22	40.8217	14.1357	0.6	1.7 ± 0.3	143
29/09/2023	00:20:39	40.8238	14.1340	0.7	1.9 ± 0.3	125
29/09/2023	21:25:07	40.8307	14.1160	2.6	1.3 ± 0.3	95
29/09/2023	21:57:58	40.8265	14.1397	2.8	2.7 ± 0.3	185
01/10/2023	13:33:09	40.8328	14.1357	2.5	2.9 ± 0.3	173
02/10/2023	20:08:26	40.8307	14.1500	2.6	4.0 ± 0.3	295
04/10/2023	08:46:55	40.8295	14.1342	2.5	2.6 ± 0.3	143
16/10/2023	10:36:21	40.8250	14.1422	2.1	3.6 ± 0.3	208
23/11/2023	18:41:46	40.8315	14.1333	2.8	3.0 ± 0.3	145

3. Results and discussion

The first method involved studying the extent of displacements and the direction and amplitude of variations measured in time intervals correspondent with the occurrence of individual seismic events, comparing them to the d_{max} and the d_{med} displacements values and to the Δd_{med} and Δd_{max} variations values respectively.

The analyses conducted did not reveal any direct correlations between the occurrence of individual earthquakes, even of significant intensity or occurring near the surveyed building, and the changes in the trend of displacement variations recorded by any of the three inclinometers. In terms of extent of the displacements, in no case were the maximum values d_{max} or other significant ones recorded in

Table 5
Average and maximum displacement variation values and average displacement values along the X and Y components of all three inclinometers for the different reference time intervals considered in both analysis methods.

Average displacement variation values *[cm]*						
Reference time intervals	**INCL_1**		**INCL_2**		**INCL_3**	
	$\Delta d_{x,med}$	$\Delta d_{y,med}$	$\Delta d_{x,med}$	$\Delta d_{y,med}$	$\Delta d_{x,med}$	$\Delta d_{y,med}$
August 08, 2023–January 23, 2024 *(reference period)*	*0,03*	*0,04*	*0,05*	*0,04*	*0,03*	*0,03*
August 08, 2023–August 14, 2023 *(first period of minor seismicity)*	*0,04*	*0,06*	*0,13*	*0,08*	*0,08*	*0,07*
August 22, 2023–September 21, 2023 *(second period of minor seismicity)*	*0,04*	*0,05*	*0,09*	*0,05*	*0,05*	*0,04*
September 30, 2023–January 23, 2024 *(third period of minor seismicity)*	*0,03*	*0,03*	*0,03*	*0,03*	*0,02*	*0,01*
August 15, 2023–August 21, 2023 *(first cluster)*	*0,04*	*0,06*	*0,21*	*0,18*	*0,10*	*0,11*
September 22, 2023–September 29, 2023 *(second cluster)*	*0,03*	*0,04*	*0,05*	*0,04*	*0,03*	*0,02*
Maximum displacement variation values *[cm]*						
Reference time intervals	**INCL_1**		**INCL_2**		**INCL_3**	
	$\Delta d_{x,max}$	$\Delta d_{y,max}$	$\Delta d_{x,max}$	$\Delta d_{y,max}$	$\Delta d_{x,max}$	$\Delta d_{y,max}$
August 08, 2023–January 23, 2024 *(reference period)*	*0,38*	*0,52*	*3,47*	*2,11*	*1,49*	*1,59*
August 08, 2023–August 14, 2023 *(first period of minor seismicity)*	*0,28*	*0,52*	*2,58*	*1,40*	*1,39*	*0,88*
August 22, 2023–September 21, 2023 *(second period of minor seismicity)*	*0,30*	*0,52*	*2,09*	*2,11*	*1,04*	*1,07*
September 30, 2023–January 23, 2024 *(third period of minor seismicity)*	*0,38*	*0,47*	*2,18*	*0,47*	*0,93*	*0,85*
August 15, 2023–August 21, 2023 *(first cluster)*	*0,24*	*0,44*	*3,47*	*2,09*	*1,49*	*1,59*
September 22, 2023–September 29, 2023 *(second cluster)*	*0,17*	*0,33*	*0,77*	*0,40*	*0,37*	*0,29*
Average displacement values *[cm]*						
Reference time intervals	**INCL_1**		**INCL_2**		**INCL_3**	
	$d_{x,med}$	$d_{y,\ med}$	$d_{x,med}$	$d_{y,\ med}$	$d_{x,med}$	$d_{y,\ med}$
August 08, 2023–January 23, 2024 *(reference period)*	*(+)0,15*	*(+)0,13*	*(+)1,61*	*(−)0,37*	*(+)0,67*	*(−)0,90*
August 08, 2023–August 14, 2023 *(first period of minor seismicity)*	*(−)0,09*	*(+)0,02*	*(+)0,60*	*(−)0,20*	*(+)0,06*	*(−)0,76*
August 22, 2023–September 21, 2023 *(second period of minor seismicity)*	*(−)0,06*	*(+)0,01*	*(+)1,31*	*(−)0,56*	*(+)0,45*	*(−)0,91*
September 30, 2023–January 23, 2024 *(third period of minor seismicity)*	*(+)0,24*	*(+)0,18*	*(+)1,82*	*(−)0,32*	*(+)0,81*	*(−)0,91*
August 15, 2023–August 21, 2023 *(first cluster)*	*(−)0,03*	*(+)0,01*	*(+)0,81*	*(−)0,40*	*(+)0,16*	*(−)0,89*
September 22, 2023–September 29, 2023 *(second cluster)*	*(+)0,05*	*(+)0,07*	*(+)1,54*	*(−)0,51*	*(+)0,62*	*(−)0,92*

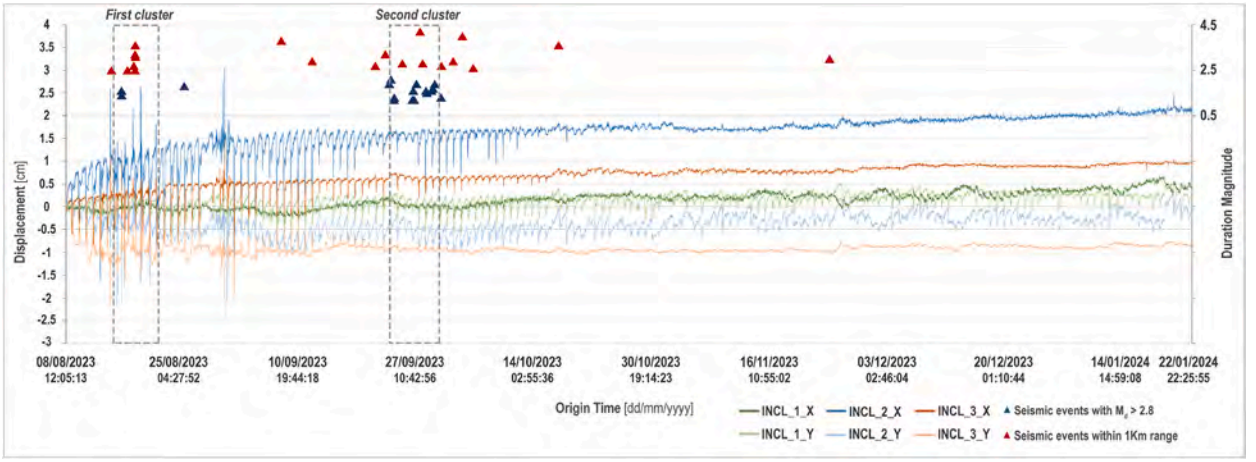

Fig. 12. Trend of displacement variations recorded by inclinometers along both X and Y reference components and indication of the 38 seismic events classified according to their Duration Magnitude along with an indication of the two time intervals related to the two clusters of events considered.

correspondence with the 38 seismic events considered, and the values observed remain consistent with the average values d_{med} of the reference time intervals in which they fall and the analysed trends. The notable changes and peaks observed for INCL_2 and INCL_3 (§ 2.2) were not registered in correspondence of any seismic events, which, in the absence of further stress, may be associated with other external factors such as temperature compensation issues.

Regarding the direction and amplitude of displacement variations, in almost all cases, there are no sudden variations in direction during or immediately after the earthquakes, nor are significant differences in amplitude variations recorded from the average Δd_{med} and maximum Δd_{max} values, either in the overall trend of the entire reference period or during periods of minor seismicity or cluster events. In case some changes were noted, a comprehensive analysis of the data registered with respect to the overall trends of

displacements was developed. When observed, the changes in direction recorded close to the events are still coherent with the cyclical patterns observed in each relevant time interval, excluding a direct correlation between the two phenomena. Similarly, when the amplitude of the variations Δd recorded at time intervals close to the event appear the be higher than the Δd_{med} and Δd_{max} values, they are only marginally higher and do not represent anomalies compared to the general pattern observed over the entire reference period, as well as over the different time intervals considered.

Moreover, the significant variations observed for INC_2 and INCL_3 in August (§ 2.2), are not limited to time intervals close to the individual seismic events, and for all three inclinometers substantial differences in variation amplitudes are in fact observed at intervals unrelated to seismic events as well as during periods of minor seismicity. This results in difficulties in establishing a direct correlation between such changes and the events themselves, and they are not attributable to the occurrence of the individual earthquake, and do not constitute an anomaly in the oscillatory trends observed.

Some examples of specific comparisons are described, deferring observations of data to an analysis of Annex B of the Supplemental Files. During the seismic events occurred on August 18, none of the three inclinometers recorded maximum displacement values d_{max} in time intervals close to the event, and the extent of displacements do not show significant changes compared to the d_{med} observed across the different time intervals (Tables 2, 5 and 6). The slightly above-average values observed (e.g., along the Y-axis for INCL_1) do not represent anomalies, as a deeper analysis of the displacement diagrams reveals they are consistent with the overall observed trends. As for the displacement variations recorded straddling of the event, no sudden changes in direction are observed for any of the three inclinometers (Table 6), and the amplitudes remain consistent with the Δd_{med} and lower than Δd_{max} across all reference time intervals (Tables 5 and 6).

Similarly, during the event on September 27th, the displacement values registered by the three inclinometers are all lower than d_{max} and aligned with trend patterns of the relevant time intervals (Tables 5 and 6). Furthermore, no variations in direction are observed between the values registered before and after the event, and no significant differences in amplitude are noted from the average Δd_{med}. The consistency of these considerations could be significant, given that, in the first case, the four seismic events occurred in close succession and were relatively high in magnitude, while the second event had the highest M_d value of the entire reference period (Table 4).

The second method involved studying the d_{med} and Δ_{dmed} displacement values registered during the clusters, comparing them to those registered during the other reference time intervals considered.

From this second analysis, the anomalies of d_{med} and Δ_{dmed} values observed during clusters of seismic events result not to be correlated to the events themselves. No differences result in comparing these values recorded during clusters and the ones referred to the entire reference period, including periods of minor seismicity.

In this case, INCL_1 behaves differently than INCL_2 and INCL_3. For INC_1, during the time intervals associated with the two clusters, no significant changes emerged in the extent of the d_{med} values either in the amplitudes of Δd_{med} values compared to the overall average trends, including those associated with periods with minor seismicity (Table 5). For INCL_2 and INCL_3, the d_{med} values recorded during the two clusters are consistent with those recorded during the other time intervals, indicating no specific influences of the high frequency of seismic events on the extents of the average displacement observed.

Regarding the Δd_{med} values, for INCL_2 and INCL_3 much higher amplitudes are observed only during the first cluster of August (Table 5). However, these differences are compatible with the relevant period of stabilisation of the building after the consolidation interventions, suggesting again there is no correlation with the occurrence of high frequency of seismic events. After this period, the displacement variations of both inclinometers tend to stabilise for both their components.

In general, the analysis of the trend of displacement variations for INCL_1 showed minimal fluctuations and changes in values with no significant average final displacements, indicating that both its X and Y components remain mainly stable over time. The analysis of the trend of displacement variations for INCL_2 and INCL_3, in contrast, shows an average final displacement, but is not correlated with the high frequency of seismic events.

Considering these average final displacement values, the building appears to have experienced a permanent resulting displacement over the entire reference period, albeit of slight magnitude. However, these values remain within the alert threshold of $\pm 1^{\circ}$, as defined by the company responsible for the monitoring plan. This threshold provides a reasonable margin to account for normal fluctuations and ensure accuracy control, having been established through experience and cross-referenced with the sensitivity of the monitoring equipment and potential external influences, such as environmental conditions and temperature variations. If values exceed this threshold, more detailed inspections and potential interventions would be promptly initiated on the monitored building to prevent further damage and safety threats.

This substantiates the results indicating that, after a period of stabilisation, the entire monitored building remained stable over time.

Discussing the results of both comparison methods, no specific correlations have been observed between the trends of displacement variations and either the occurrence of individual seismic events or clusters of events. The more pronounced fluctuations observed between August and September, could be therefore attributed to a combination of the following conditions: the building's stabilisation period following interventions, which were mostly localised near the cantonment were INCL_1 was installed, indicating the differing behaviours of the other two inclinometers; the rapid diurnal temperature transitions during these months (§ 2.2), occurring within higher temperature ranges, to which the monitoring system could be more vulnerable and, therefore, could have been affected more than during the others; other environmental or external factors. The analysis carried out indicates that the seismic component of the Bradyseism, in the range of low intensity, does not affect the building in terms of final permanent displacement.

The latter may be related to temperature compensation issues influencing the inclinometers combined with the effects of soil deformation, that constitutes the second component of bradyseismic phenomena. According to the proposed map in Fig. 13, it is easy to

Table 6
Displacement values and variations recorded in time intervals close to the occurrence of two of the considered seismic events for all three inclinometers.

Date *[dd/mm/yyyy]*	Seismic event	Measurement	Displacement values *[cm]*						Displacement variations *[cm]*					
	Time *[UTC]*		INCL_1		INCL_2		INCL_3		INCL_1		INCL_2		INCL_3	
			d_x	d_y	d_x	d_y	d_x	d_y	Δd_x	Δd_y	Δd_x	Δd_y	Δd_x	Δd_y
August 18, 2023	04:09:59	03:52:41	*(+)0,00*	*(+)0,21*	*(+)1,08*	*(−)0,30*	*(+)0,25*	*(−)0,85*	*0,02*	*0,05*	*0,10*	*0,07*	*0,06*	*0,00*
	04:10:30													
	04:18:05	04:23:05	*(+)0,02*	*(+)0,16*	*(+)0,19*	*(-)0,23*	*(+)0,31*	*(-)0,85)*						
	04:22:49													
September 27, 2023	01:35:34	01:11:11	*(+)0,00*	*(+)0,10*	*(+)1,61*	*(−)0,47*	*(+)0,64*	*(−)0,92*	*0,05*	*0,00*	*0,05*	*0,00*	*0,01*	*0,01*
		01:40:51	*(+)0,05*	*(+)0,10*	*(+)1,66*	*(−)0,47*	*(+)0,65*	*(−)0,91*						

understand that the differential increase in height reached in each area of the caldera determines a slight inclination of the soil, that might be compatible with a subsequent relative displacement of buildings located in the relevant area.

From these observations, it can be discussed that the impact of low-intensity and high-frequency solicitations, typical of bradyseismic phenomena, do not significantly affect the building's behaviour in terms of local or cumulative effects on the technical elements of the Load-bearing Structure.

However, significant disparities were observed between the average displacement values of INCL_1 and those of INCL_2 and INCL_3, both in terms of directions and extent. This might be due to the fact that the three inclinometers were installed at different positions on the façade, subjected to differential deformations due to the subsidence of the foundation soil and the broader soil deformation component of Bradyseism. These types of deformations, as well as those associated with the other extensive hazards deriving from the surrounding context, are not compatible with the vulnerability of the technical elements of the façade, resulting in much more significant impacts on these elements.

The results of both analysis methods and the direct observation of the evolution of the anomalies on the façade, showed the stabilisation of the prevalent crack patterns after the consolidation interventions (Fig. 3).

Since the prevalent crack pattern was attributed to the subsidence, while the other façade's anomalies were pre-existent and were not significantly increased by specific bradyseismic phenomena occurred in the analysed period, a wider investigation was carried out to interpret their evolution over time.

The assessment of the state of preservation of the vulnerable technical elements considered was carried out through the comparison of archival satellite images of the building obtained from the online mapping and navigation service "Google Street View". The analysis covered the years from 2008, that represents the earliest available reference in Google's historical archive, to 2023, with all available images being examined to capture the progressive deterioration of the building envelope over time. The images presented in Fig. 14 were selected to illustrate the progressive deterioration in correspondence with key time intervals supporting the considerations drawn from the analysis. The first three-time intervals together show minimal progressive deterioration in the state of preservation of the building envelope, while the later images reveal, over a shorter period, a more rapid and notable increase in degradation particularly since 2018, corresponding to the intensification of bradyseismic phenomena. Therefore, it is reasonable to link the amplification of these anomalies to the impacts of seismic-deformation phenomena of the Bradyseism, in the long term, on the vulnerable technical elements of the building envelope. These impacts, combined with other extensive hazards, exacerbate the natural deterioration of the envelope elements, resulting in significant effects on their integrity and performance.

This state of preservation of façades and the related vulnerability of technical elements, mainly due to seismic deformation phenomena linked to Bradyseism still determine a hazardous condition for the urban context, even after the stabilisation of the Load-Bearing structure. In this view, the impact of Building Risk can be easily understood and qualitatively appreciated as an additional risk scenario affecting streets and people exposed.

4. Conclusions and future developments

The described research provides a significant assessment of the importance of the vulnerability of technical elements of the envelope in Bradyseismic risk scenarios. The analysis carried out demonstrated that with the intensification of bradyseismic stresses in the range of low intensity and high frequency, the technical elements of the Load-bearing Structure did not pose a significant risk to the urban system, whereas the technical elements of the building envelope had a much more substantial impact in terms of Building Risk. With this in mind, the Building Risk can be considered as an additional factor in the multi-risk scenario of Campi Flegrei, mainly characterized by volcanic and seismic hazards, floods, environmental exposition (especially related to the impact of chloride salts in the areas near the sea, and sulphates salts in the inner areas, near the Solfatara) and climate change. Considering the influence of Building risk on urban systems, the conclusion of the emergency phase was declared by the Public Administration only after the splitting of degraded finishings of the technical elements of the façade. Future research developments aim to overcome some of the critical issues that emerged in the conducted study, which mainly pertain to the unavailability of data on the components of deformation and ground accelerations at the scale of the building or building aggregate.

Although the analysis conducted did not show direct effects of the seismic deformation stresses linked to Bradyseism, in terms of detachments and falling parts within the analysed period, significant economic, social, infrastructural, functional, and safety impacts were recorded on the urban context. Managing the emergency, across all its phases, imposed substantial burdens for the Public Administration and private individuals to cope with, among others, the costs associated with temporary housing relocation for affected individuals, the interruption of commercial activities, the reorganization of vehicular circulation, and limited access to essential services. The impacts on the community were also recorded in terms of the perception of safety, testifying the importance of designing suitable risk communication strategies aimed at mitigating the overall state of agitation of the population called upon to live with this kind of recurring event. In this regard, the methodological approach adopted in the research conducted by the authors, along with the elaborated results, provide valuable data to convey a positive message to the population regarding the actions implemented by the Public Administration.

Given the limited availability of literature-based data on Building Risk evaluation, the ongoing developments of this research aim at collecting more experimental data. In this perspective, the challenge consists of elaborating innovative vulnerability models to describe and predict the behaviour of the technical elements of façades, considering that existing models thought for the assessment of Load-bearing Structure elements' vulnerability cannot be applied.

Experimental approaches, aimed at comprehensively understanding this risk factor in urban contexts, cannot disregard a preliminary knowledge of the state of preservation of the building envelopes. This understanding must be further enhanced through

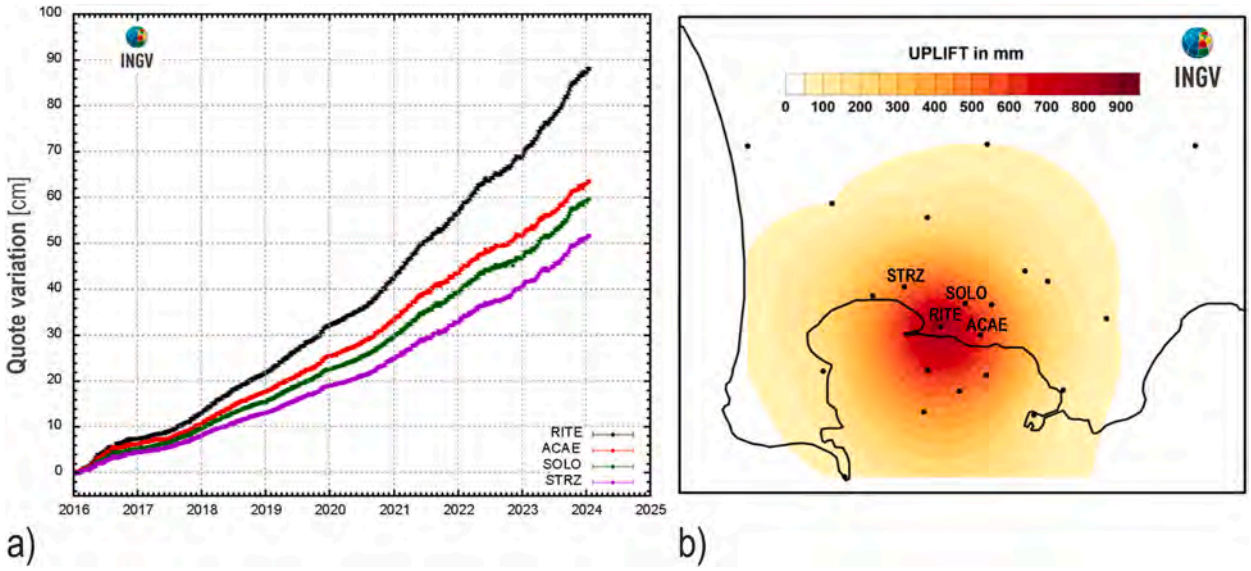

Fig. 13. Indication of the soil deformation phenomenon registered in the Campi Flegrei area. a) Time series of weekly elevation changes of RITE (Pozzuoli - Rione Terra), ACAE (Accademia Aeronautica), SOLO (Solfatara) and STRZ (Pozzuoli - Cemetery) stations from January 2016 to January 2024; b) Map of horizontal vertical GNSS displacements recorded from January 2016 to January 2024. Images curated by © Osservatorio Vesuviano and adapted from the monitoring bulletin released in January 2024 [84].

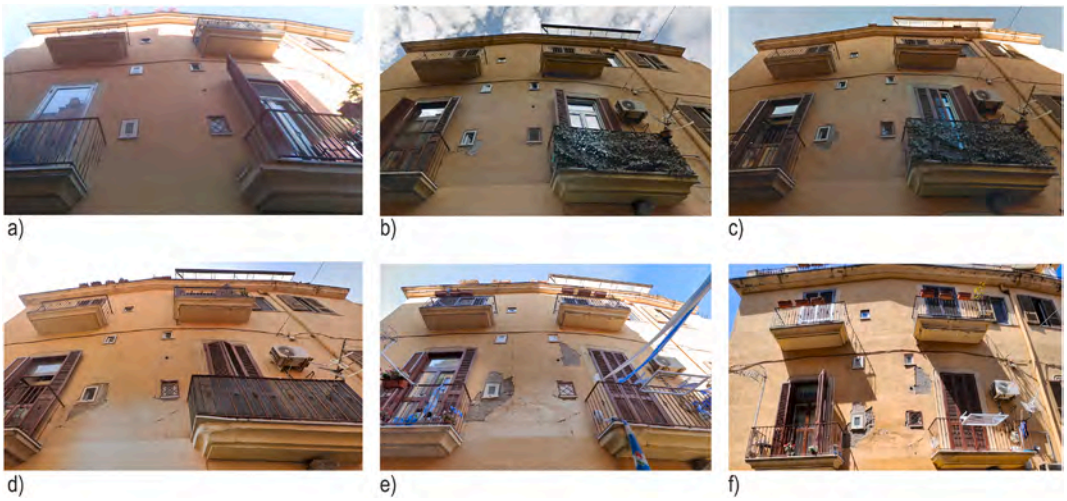

Fig. 14. Evolution of the state of preservation of the technical elements of the building envelope. a) Image dated April 2008; b) Image dated August 2012; c) Image dated August 2016; d) Image dated October 2018; e) Image dated April 2023. Retrieved from © Google Maps Street View. f) Image dated August 2023. © Authors.

monitoring phases aimed at interpreting the evolution of this state preservation over time, considering the multi-hazard scenario typical of the analysed context.

These lines of research development align with the emergency management planning mandates outlined at the national level through the Campi Flegrei Decree-Law of October 12, 2023 [85]. The Decree, absorbing the findings of the studies conducted by the authors in support of the Public Administrations of the Phlegraean area, emphasizes the importance of gaining a comprehensive understanding and in-depth knowledge of the state of preservation of the built environment, paying renewed attention to the analysis of the vulnerabilities of the technical elements of the envelope and the assessment of the relevant Building Risk. In this regard, the relevance of the themes developed extends beyond the advancement of scientific knowledge to the development of methodologies for implementing operational strategies aimed at mitigating Building Risk and enhancing urban resilience.

The methodological approach holds broad applicability in studying the impacts on the built environment caused by low-intensity and high-frequency forcings common in urbanized settings in any type of multi-risk scenario. For instance, it can be applied to assess the stresses exerted on building envelopes by infrastructure systems such as roads, railways, and subways, or by meteorological events exacerbated by the effects of climate change.

Funding

This contribution reports the results of the studies carried out within the RETURN Extended Partnership and received funding from the European Union Next-GenerationEU (National Recovery and Resilience Plan – NRRP, Mission 4, Component 2, Investment 1.3 – D. D. 1243 August 2, 2022, PE0000005).

CRediT authorship contribution statement

Mariacarla Fraiese: Writing – original draft, Visualization, Methodology, Investigation, Data curation. **Veronica Vitiello:** Conceptualization, Investigation, Validation, Visualization, Writing – original draft, Writing - review & editing. **Roberto Castelluccio:** Writing – review & editing, Validation, Supervision, Methodology, Conceptualization.

Declaration of competing interest

The authors declare the following financial interests/personal relationships which may be considered as potential competing interests:Roberto Castelluccio reports financial support was provided by European Union Next-GenerationEU. If there are other authors, they declare that they have no known competing financial interests or personal relationships that could have appeared to influence the work reported in this paper.

Data availability

Data will be made available on request.

Acknowledgements

The authors would like to thank TECNO IN Geosolution S.p.A. for providing the inclinometric monitoring service of the surveyed building and for supplying the technical data that were processed and analysed within the scope of this contribution.

Appendix A. Supplementary data

Supplementary data to this article can be found online at https://doi.org/10.1016/j.ijdrr.2024.104899.

References

[1] G. Orsi, S. de Vita, M.A. Di Vito, The restless, resurgent Campi Flegrei nested caldera (Italy): constraints on its evolution and configuration, J. Volcanol. Geoth. Res. 74 (1996) 179–214, https://doi.org/10.1016/S0377-0273(96)00063-7.
[2] G. Orsi, L. Civetta, C. Del Gaudio, S. de Vita, M.A. Di Vito, R. Isaia, S. Petrazzuoli, G. Ricciardi, C. Ricco, Short-term ground deformations and seismicity in the nested Campi Flegrei Caldera (Italy): an example of active block resurgence in a densely populated area, J. Volcanol. Geoth. Res. 91 (1999) 415–451, https://doi.org/10.1016/S0377-0273(99)00050-5.
[3] M.A. Di Vito, R. Isaia, G. Orsi, J. Southon, S. de Vita, M. D'Antonio, L. Pappalardo, M. Piochi, Volcanism and deformation in the past 12 ka at the Campi Flegrei caldera (Italy), J. Volcanol. Geoth. Res. 91 (1999) 221–246, https://doi.org/10.1016/S0377-0273(99)00037-2.
[4] G. Orsi, M.A. Di Vito, R. Isaia, Volcanic hazard assessment at the restless Campi Flegrei caldera, Bull. Volcanol. 66 (2004) 514–530, https://doi.org/10.1007/s00445-003-0336-4.
[5] V. Di Rienzo, I. Arienzo, L. Civetta, M. D'Antonio, S. Tonarini, M.A. Di Vito, G. Orsi, The magmatic feeding system of the Campi Flegrei caldera: architecture and temporal evolution, Chem. Geol. 281 (2011) 227–241, https://doi.org/10.1016/j.chemgeo.2010.12.010.
[6] M. Di Vito, V. Acocella, G. Aiello, D. Barra, M. Battaglia, A. Carandente, C. Del Gaudio, S. de Vita, G.P. Ricciardi, C. Ricco, R. Scandone, F. Terrasi, Magma transfer at Campi Flegrei caldera (Italy) before the 1538 AD eruption, Sci. Rep. 6 (2016), https://doi.org/10.1038/srep32245.
[7] C. Del Gaudio, I. Aquino, G.P. Ricciardi, C. Ricco, R. Scandone, Unrest episodes at Campi Flegrei: a reconstruction of vertical ground movements during 1905-2009, J. Volcanol. Geoth. Res. 195 (2010) 48–56, https://doi.org/10.1016/j.jvolgeores.2010.05.014.
[8] A. Bevilacqua, A. Neri, P. De Martino, R. Isaia, A. Novellino, F.D.A. Tramparulo, S. Vitale, Radial interpolation of GPS and leveling data of ground deformation in a resurgent caldera: application to Campi Flegrei (Italy), J. Geodesy 94 (2020) 1–27, https://doi.org/10.1007/s00190-020-01355-x.
[9] A. Lima, R.J. Bodnar, B. De Vivo, F.J. Spera, H.E. Belkin, Interpretation of recent unrest events (bradyseism) at Campi flegrei, Napoli (Italy): comparison of models based on cyclical hydrothermal events versus shallow magmatic intrusive events, Geofluids (2021), https://doi.org/10.1155/2021/2000255, 2021.
[10] C. Ricco, S. Petrosino, I. Aquino, C. Del Gaudio, M. Falanga, Some investigations on a possible relationship between ground deformation and seismic activity at Campi flegrei and ischia volcanic areas (southern Italy), Geosciences 9 (5) (2019), https://doi.org/10.3390/geosciences9050222.
[11] P. De Martino, M. Dolce, G. Brandi, G. Scarpato, U. Tammaro, The ground deformation history of the neapolitan volcanic area (Campi flegrei caldera, somma–vesuvius volcano, and ischia island) from 20 years of continuous gps observations (2000–2019), Rem. Sens. 13 (14) (2021), https://doi.org/10.3390/rs13142725.
[12] S. Vitale, J. Natale, Combined volcano-tectonic processes for the drowning of the Roman western coastal settlements at Campi Flegrei (southern Italy), Earth Planets Space 75 (38) (2023), https://doi.org/10.1186/s40623-023-01795-7.
[13] G. De Natale, C. Troise, F. Pingue, G. Mastrolorenzo, L. Pappalardo, M. Battaglia, E. Boschi, The Campi Flegrei caldera: unrest mechanisms and hazards, in: C. Troise, G. De Natale, C.R.J. Kilburn (Eds.), Mechanisms of Activity and Unrest at Large Calderas, vol. 269, Geological Society, London, Special Publications, 2006, pp. 25–45, https://doi.org/10.1144/GSL.SP.2006.269.01.03.
[14] F. Pingue, S.M. Petrazzuoli, F. Obrizzo, U. Tammaro, P. De Martino, G. Zuccaro, Monitoring system of buildings with high vulnerability in presence of slow ground deformations (The Campi Flegrei, Italy, case), Measurement 44 (2011) 1628–1644, https://doi.org/10.1016/j.measurement.2011.06.015.
[15] M. Calò, A. Tramelli, Anatomy of the Campi flegrei caldera using enhanced seismic tomography models, Sci. Rep. 8 (2018), https://doi.org/10.1038/s41598-018-34456-x.
[16] F. Scotto di Uccio, A. Lomax, J. Natale, T. Muzellec, G. Festa, S. Nazeri, V. Convertito, A. Bobbio, C. Strumia, A. Zollo, Delineation and Fine-Scale Structure of Active Fault Zones during the 2014-2023 Unrest at the Campi Flegrei Caldera (Southern Italy) from High-Precision Earthquake Locations, ESS Open Archive, 2024, https://doi.org/10.22541/essoar.170224505.51315564/v1. (Accessed 10 December 2023).

[17] Presidenza del Consiglio dei Ministri, Dipartimento di Protezione Civile. Istituto Nazionale di Geofisica e Vulcanologia. Sezione di Napoli, Osservatorio Vesuviano (curated by), Bollettino di Sorveglianza Campi Flegrei - Marzo, 2024.

[18] Presidenza del Consiglio dei Ministri, Dipartimento di Protezione Civile. Rischi – Campi Flegrei. Retrieved from https://rischi.protezionecivile.gov.it/it/vulcanico/vulcani-italia/campi-flegrei/. Last accessed November 10th, 2023.

[19] C. Troise, G. De Natale, R. Schiavone, R. Somma, R. Moretti, The Campi Flegrei caldera unrest: discriminating magma intrusions from hydrothermal effects and implications for possible evolution, Earth Sci. Rev. (108) (2019) 108–122, https://doi.org/10.1016/j.earscirev.2018.11.007.

[20] Presidenza del Consiglio dei Ministri. Dipartimento della Protezione Civile, D.P.C.M. 24 Giugno 2016 - Disposizioni per l'aggiornamento della pianificazione di emergenza per il rischio vulcanico dei Campi Flegrei, Accessible at, https://www.protezionecivile.gov.it/static/7cec46f0e45c7502a24ea51017929b66/dpcm-24-giugno-2016-campi-flegrei.pdf, 2016.

[21] Presidenza del Consiglio dei Ministri, Dipartimento di Protezione Civile. Livelli di allerta. Retrieved from https://www.protezionecivile.gov.it/en/approfondimento/livelli-di-allerta–versione-inglese-/#:~:text=il%20livello%20di%20allerta%20giallo,di%20forte%20disequilibrio%20del%20vulcano.

[22] F.L. Perelli, L.S. Di Maio, D. De Gregorio, G. Magliulo, P. De Martino, G. Zuccaro, Impact assessment caused by bradyseism phenomena in the Campi Flegrei area, Frontiers in Built Environment 9 (2023), https://doi.org/10.3389/fbuil.2023.1129175.

[23] Presidenza del Consiglio dei Ministri, Dipartimento di Protezione Civile. Istituto Nazionale di Geofisica e Vulcanologia. Sezione di Napoli, Osservatorio Vesuviano (curated by), Bollettino di Sorveglianza Campi Flegrei - Agosto, 2023.

[24] Presidenza del Consiglio dei Ministri, Dipartimento di Protezione Civile. Istituto Nazionale di Geofisica e Vulcanologia. Sezione di Napoli, Osservatorio Vesuviano (curated by), Bollettino di Sorveglianza Campi Flegrei - Settembre, 2023.

[25] Terremoto a Pozzuoli, solo ad agosto 609 eventi nell'area flegrea". Napoli, Il Mattino. Accessible at: https://www.ilmattino.it/pay/edicola/terremoto_scosse_pozzuoli_609_eventi_agosto-7586840.html.

[26] T. Ricci, F. Barberi, M.S. Davis, R. Isaia, R. Nave, Volcanic risk perception in the Campi Flegrei area, J. Volcanol. Geoth. Res. 254 (2013) 118–130, https://doi.org/10.1016/j.jvolgeores.2013.01.002.

[27] G. Zuccaro, D. De Gregorio, Impact assessments in volcanic areas – the Vesuvius and Campi Flegrei cases studies, Ann. Geophys. 62 (1) (2019) 1–18, https://doi.org/10.4401/ag-7827.

[28] D. Charlton, C. Kilburn, S. Edwards, Volcanic unrest scenarios and impact assessment at Campi Flegrei caldera, Southern Italy, Journal of Applied Volcanology 9 (7) (2020), https://doi.org/10.1186/s13617-020-00097-x.

[29] F. Curcio, Il piano per la popolazione, in: O. Ragone, C. Sannino (Eds.), *Campi Flegrei. Tra I Fuochi Della Storia*. Collana Novanta-Venti, La Repubblica. Napoli: Ed. Guida Editori S.r.L, 2023.

[30] M. Mariani, F. Pugi, Sequenza sismica dei Campi Flegrei: studi su accelerazioni, jerk e possibili effetti sulle costruzioni per accumulo del danno (2023). Retrieved from, https://www.ingenio-web.it/articoli/sequenza-sismica-dei-campi-flegrei-studi-su-accelerazioni-jerk-e-possibili-effetti-sulle-costruzioni-per-accumulo-del-danno/.

[31] D. Johnston, B. Scott, B. Houghton, D. Paton, D. Dowrick, P. Villamor, J. Savage, Social and economic consequences of historic caldera unrest at the Taupo volcano, New Zealand and the management of future episodes of unrest, Bull. N. Z. Soc. Earthq. Eng. 35 (4) (2002) 215–230, https://doi.org/10.5459/bnzsee.35.4.215-230.

[32] S. Carlino, Review article: brief history of volcanic risk in the Neapolitan area (Campania, southern Italy): a critical review, Nat. Hazards Earth Syst. Sci. 21 (2021) 3097–3112, https://doi.org/10.5194/nhess-21-3097-2021.

[33] United Nations General Assembly, Report of the Open-Ended Intergovernmental Expert Working Group on Indicators and Terminology Relating to Disaster Risk reduction. Geneva, Switzerland, 2016. https://www.preventionweb.net/quick/11605. (Accessed 21 December 2023).

[34] R. Castelluccio, M. Fraiese, V. Vitiello, L. Diana, L'identificazione del Rischio Edilizio come fase necessaria per la gestione degli scenari multi-rischio, in: Proceedings of Colloqui.AT.e 2023, Convegno Ar.Tec, Bari, Edicom Edizioni, 2023. ISBN 979-12-81229-02-0.

[35] R. Castelluccio, Il costruito come fattore di rischio, TECHNE - Journal of Technology for Architecture and Environment 15 (2018) 225–233, https://doi.org/10.13128/Techne-22110.

[36] A. Silva, J. de Brito, Service life of building envelopes: a critical literature review, J. Build. Eng. 44 (2021), https://doi.org/10.1016/j.jobe.2021.102646.

[37] J. Barrelas, Q. Ren, C. Pereira, Implications of climate change in the implementation of maintenance planning and use of building inspection systems, J. Build. Eng. 40 (2021), https://doi.org/10.1016/j.jobe.2021.102777.

[38] S. Taghavi, E. Miranda, Response assessment of nonstructural building elements. PEER report 2003/05, The Pacific Earthquake Engineering Research Center, Berkeley, CA (2003). December 10th, 2023, from, https://peer.berkeley.edu/sites/default/files/0305_s._taghavi_e._miranda_.pdf.

[39] Federal Emergency Management Agency. Department of Homeland Security, Earthquake hazard mitigation for nonstructural elements, FEMA 74 Field Manual (2005). https://mitigation.eeri.org/files/FEMA74_FieldManual.pdf. (Accessed 15 December 2023).

[40] Presidenza del Consiglio dei Ministri. Dipartimento della Protezione Civile, Linee Guida per la riduzione della vulnerabilità di elementi non strutturali, arredi e impianti (2009). December 28th, from, https://download.acca.it/BibLus-net/ApprofondimentiTecnici/LG_NStrutturali.pdf.

[41] V. Convertito, A. Zollo, Assessment of pre-crisis and syn-crisis seismic hazard at Campi Flegrei and Mt. Vesuvius volcanoes, Campania, southern Italy, Bullettin of Volcanology 73 (6) (2011) 767–783, https://doi.org/10.1007/s00445-011-0455-2.

[42] S. Bianchi, J. Ciurlanti, S. Pampanin, Seismic vulnerability of non-structural components: from traditional solutions to innovative low-damage systems, in: In Proceedings of SECED Conference, Earthquake Risk and Engineering towards a Resilient World, 2019. Greenwich, London, https://hdl.handle.net/11573/1346110.

[43] D. Perrone, P.M. Calvi, R. Nascimbene, E.C. Fischer, G. Magliulo, Seismic performance of non-structural elements during the 2016 Central Italy earthquake, Bull Earthquake Eng 17 (2019) 5655–5677, https://doi.org/10.1007/s10518-018-0361-5.

[44] C. Del Gaudio, M.T. De Risi, S.A. Scala, G.M. Verderame, Seismic loss estimation in pre-1970 residential RC buildings: the role of infills and services in low–mid-rise case studies, Frontiers in Built Environment 6 (2020), https://doi.org/10.3389/fbuil.2020.589230.

[45] G.J. O'Reilly, G.M. Calvi, A seismic risk classification framework for non-structural elements, Bull. Earthq. Eng. 19 (2021) 5471–5494, https://doi.org/10.1007/s10518-021-01177-y.

[46] R. Castelluccio, D. Di Martire, L. Guerriero, V. Vitiello, Methods for assessing the vulnerability of non-structural components. Monitoring for risk management, Sustainable Mediterranean Construction (SMC) 14 (2021) 156–162. ISSN Online: 2420-8213.

[47] M. Zito, R. Nascimbene, P. Dubini, D. D'Angela, G. Magliulo, Experimental seismic assessment of nonstructural elements: testing protocols and novel perspectives, Buildings 12 (2022), https://doi.org/10.3390/buildings12111871.

[48] R. Castelluccio (Ed.), Studio degli scenari di rischio a supporto del Piano di Protezione Civile del Comune di Pozzuoli, first ed., 2017. Napoli: Ed. Doppiavoce).

[49] S. Moghtadernejad, S. Mirza, Performance of building facades, in: Presented at the Proceedings of CSCE - 4th International Structural Specialty Conference, Canadian Society for Civil Engineers, Halifax, NS, 2014, pp. 28–31. May.

[50] G. Ruggiero, R. Marmo, M.A. Nicolella, Methodological approach for assessing the safety of historic buildings' façades, Sustainability 13 (2021) 2812, https://doi.org/10.3390/su13052812.

[51] W. Castro, J. Souza, P. Gaspar, A. Silva, Mapping the risk of occurrence of defects in façades with ceramic claddings, Buildings 13 (2023), https://doi.org/10.3390/buildings13051209.

[52] J.L. Erdly, T.A. Schwartz (Eds.), Building Façade Maintenance, Repair and Inspection, ASTM International, West Conshohocken, PA, 2004.

[53] L. Manzoni, Resilienza puteolana, in: O. Ragone, C. Sannino (Eds.), *Campi Flegrei. Tra I Fuochi Della Storia*. Collana Novanta-Venti, La Repubblica. Napoli: Ed. Guida Editori S.r.L, 2023.

[54] G. Macedonio, M. Martini, A. Neri, P. Papale, M. Rosi, G. Zuccaro, Rapporto finale del Gruppo di Lavoro incaricato della definizione dello scenario di riferimento per il piano di emergenza dei Campi Flegrei per il rischio vulcanico per il Dipartimento della Protezione Civile. Roma, 2012, p. 31, dicembre.

[55] J.C. Gaillard, Alternative paradigms of volcanic risk perception: the case of Mt. Pinatubo in the Philippines, J. Volcanol. Geotherm. Res. 172 (2008), https://doi.org/10.1016/j.jvolgeores.2007.12.036.

[56] A. Scolobig, N. Komendantova, A. Patt, C. Vinchon, D. Monfort-Climent, M. Begoubou-Valerius, P. Gasparini, A. Di Ruocco, Multi-risk governance for natural hazards in Naples and Guadeloupe, Nat. Hazards 73 (2014), https://doi.org/10.1007/s11069-014-1152-1.
[57] Smart Mature Resilience, European project SMR. European union's horizon 2020 research and innovation programme. European Resilience Management Guideline Report, 2018. https://smr-project.eu/fileadmin/user_upload/Documents/Resources/WP_5/D5.9.SMR_European_Resilience_Management_Guideline.pdf. (Accessed 13 March 2024).
[58] UN-ISDR, Towards national resilience: good practices of national platforms for disaster risk reduction. United Nations Secretariat of the International Strategy for Disaster Reduction. Geneva, Switzerland, 2008. April 12th, 2023 from, https://www.unisdr.org/files/3292_TowardsNationalResilience.pdf.
[59] G. Cerè, Y. Rezgui, W. Zhao, Critical review of existing built environment resilience frameworks: directions for future research, Int. J. Disaster Risk Reduc. 25 (2017) 173–189, https://doi.org/10.1016/j.ijdrr.2017.09.018.
[60] K. Rus, V. Kilar, D. Koren, Resilience assessment of complex urban systems to natural disasters: a new literature review, Int. J. Disaster Risk Reduc. 31 (2018) 311–330, https://doi.org/10.1016/j.ijdrr.2018.05.015.
[61] Bradisismo a Pozzuoli, sgomberati quattro palazzi". Napoli, Corriere del Mezzogiorno. Accessible at: https://napoli.corriere.it/notizie/cronaca/23_luglio_31/bradisismo-a-pozzuoli-sgomberati-quattro-palazzi-ff5334aa-e648-4aed-81f5-2a405fbc1xlk.shtml?refresh_ce.
[62] Osservatorio Vesuviano - Istituto Nazionale di Geofisica and Vulcanologia. Accessible at https://www.ov.ingv.it/.
[63] UNI 8290-1, Edilizia residenziale. Sistema tecnologico, Analisi dei requisiti (1983).
[64] Ministero Infrastrutture e Trasporti, D.M. 17 gennaio 2018, n. 42, Norme Tecniche per le Costruzioni (NTC) (2018).
[65] A. Baglioni, A. Gottfried (Eds.), Manuale di progettazione edilizia vol.4 - Tecnologie: requisiti, soluzioni, esecuzione, prestazioni. Milano: Ed. Hoepli, 1995. ISBN 8820319810.
[66] C. Pereira, E. Hamadyk, A. Silva, Probabilistic analysis of the durability of architectural concrete surfaces, Appl. Math. Model. (77) (2020) 199–2015, https://doi.org/10.1016/j.apm.2019.07.031.
[67] R. Ramos, A. Silva, J. de Brito, P.D. Gaspar, Methodology for the service life prediction of ceramic claddings in pitched roofs, Construct. Build. Mater. 166 (2018) 386–399, https://doi.org/10.1016/j.conbuildmat.2018.01.111.
[68] A. Filiatrault, Seismic design of nonstructural building components: the new frontier of earthquake engineering, in: Proceedings of Australian Earthquake Engineering Society Virtual Conference, 2020, pp. 1–8. November 18-20, 2020.
[69] A.Z.M. Gunawan, A.Y. Saptari, H.F. Suhandri, N.A. Khalifa, K.N.M. Yunus, Literature study of building verticality monitoring analysis using GNSS and triaxial tiltmeter data integration, Jurnal Kejuruteraan 33 (4) (2021) 927–934, https://doi.org/10.17576/jkukm-2021-33(4)-15.
[70] Z. Ma, J. Choi, H. Sohn, Structural displacement sensing techniques for civil infrastructure: a review, Journal of Infrastructure Intelligence and Resilience 2 (3) (2023), https://doi.org/10.1016/j.iintel.2023.100041.
[71] L. Hui, O.U. Jinping, Structural health monitoring: from sensing technology stepping to health diagnosis, Procedia Eng. 14 (2011) 753–760, https://doi.org/10.1016/j.proeng.2011.07.095.
[72] Istituto Nazionale di Geofisica e Vulcanologia (INGV). Sezione di Napoli – Osservatorio Vesuviano. Localizzazioni Sismiche Vulcani Campani. Generator of Serenade StatIc Pages v. 5.2.2 (GOSSIP). Retrieved from https://terremoti.ov.ingv.it/gossip/, last accessed January 3rd, 2023.
[73] T. Colletta, Supplemento di Storia dell'Urbanistica", Campania, Edizioni Kappa, Luglio-Dicembre I (1988) 31.
[74] ISTAT, 154° Censimento della Popolazione e delle Abitazioni, Available at: https://www.istat.it/, 2011.
[75] H.B. Xiong, J.X. Cao, F.L. Zhang, Inclinometer based method to monitor displacement of high-rise buildings, Structural Monitoring and Maintenance 5 (1) (2018) 111–127, https://doi.org/10.12989/smm.2018.5.1.111.
[76] G.E. Green, P.E. Mikkelsen, Deformation measurements with inclinometers, Transportation Research Record (1169), Geotechnical Instrumentation (1988). Accessible at: http://onlinepubs.trb.org/Onlinepubs/trr/1988/1169/1169-001.pdf.
[77] I. Glot, I. Shardakow, A. Shestakov, R. Tsvetkov, G. Gusev, Inclinometer-based long-term monitoring of the headframe of salt mine shaft, in: Journal of Physics: Conference Series, 2021, https://doi.org/10.1088/1742-6596/1945/1/012009, 1945. XXII Winter School on Continuous Media Mechanics (WSCMM 2021) 22-26 March 2021, Perm, Russia.
[78] S. Wierzbicki, Z. Pióro, M. Osiniak, E. Antoszkiewicz, Inclinometer method of displacement measurements as an alternative to optical measurements in structural health monitoring — laboratory tests, Arch. Civ. Eng. 66 (2) (2020) 147–164, https://doi.org/10.24425/ace.2020.131802.
[79] Presidenza del Consiglio dei Ministri, Dipartimento di Protezione Civile. Istituto Nazionale di Geofisica e Vulcanologia. Convenzione Attuativa per le Attività di Servizio in esecuzione all'Accordo Quadro tra il Dipartimento della Protezione Civile e l'Istituto Nazionale di Geofisica e Vulcanologia (periodo 2022-2025). Capitolo 4 – Allegato Tecnico. Accessible at https://istituto.ingv.it/images/Accordi-dpc/Convenzione_INGV_2022-2024.pdf.
[80] S. Del Mese, L. Graziani, F. Meroni, V. Pessina, A. Tertulliani, Considerations on using MCS and EMS-98 macroseismic scales for the intensity assessment of contemporary Italian earthquakes, Bull. Earthq. Eng. 21 (2023) 4167–4189, https://doi.org/10.1007/s10518-023-01703-0.
[81] G. Grunthal, European Macroseismic Scale (EMS-98), vol. 15, Conseil de l'Europe, Cahiers du Centre Européen de Géodynamique et de Séismologie, Luxembourg, 1998.
[82] A. Sandoli, G. Brandonisio, G.P. Lignola, A. Prota, G. Fabbrocino, Seismic fragility matrices for large scale probabilistic structural safety assessment, Soil Dynam. Earthq. Eng. 171 (2023), https://doi.org/10.1016/j.soildyn.2023.107963.
[83] I. Iervolino, Terremoti e costruzioni, in: O. Ragone, C. Sannino (Eds.), *Campi Flegrei. Tra I Fuochi Della Storia*. Collana Novanta-Venti, La Repubblica. Napoli: Ed. Guida Editori S.r.L, 2023.
[84] Presidenza del Consiglio dei Ministri, Dipartimento di Protezione Civile. Istituto Nazionale di Geofisica e Vulcanologia. Sezione di Napoli, Osservatorio Vesuviano (curated by), Bollettino di Sorveglianza Campi Flegrei - Gennaio, 2024.
[85] D.L. 12/10/2023, n. 140 "Misure urgenti di prevenzione del rischio sismico connesso al fenomeno bradisismico nell'area dei Campi Flegrei". Accessible athttps://www.gazzettaufficiale.it/eli/id/2023/12/11/23A06824/sg.